CASS Report #94-3-01

Analysis of Mesospheric Winds and Waves

by

Kent L. Miller and Robert G. Roper

May 1994

Final Report: Airforce Office of Scientific Research
Contract #F49620-93-1-0460

UTAH STATE UNIVERSITY

CENTER FOR ATMOSPHERIC AND SPACE SCIENCES
UTAH STATE UNIVERSITY • LOGAN • UTAH • 84322

REPORT DOCUMENTATION PAGE

Form Approved
OMB No. 0704-0188

1. AGENCY USE ONLY *(Leave blank)*	2. REPORT DATE	3. REPORT TYPE AND DATES COVERED
	May 5, 1994	Final Report 1 Sept. 93 - 31 Dec. 93

4. TITLE AND SUBTITLE

Analysis of Mesospheric Winds and Waves

5. FUNDING NUMBERS

F49620-93-1-0460

61102F

2310 - CS

6. AUTHOR(S)

Kent L. Miller and Robert G. Roper

7. PERFORMING ORGANIZATION NAME(S) AND ADDRESS(ES)

Center for Atmospheric & Space Sciences
Utah State University
Logan, UT 84322-4405

8. PERFORMING ORGANIZATION REPORT NUMBER

AFOSR-TR- 94 0340
CASS Report #94-3-01

AFOSR-TR- 94 0340

9. SPONSORING/MONITORING AGENCY NAME(S) AND ADDRESS(ES)

AFOSR/NL
110 Duncan Avenue Suite B115
Bolling AFB, DC 20332-0001
Maj Krell

10. SPONSORING/MONITORING AGENCY REPORT NUMBER

11. SUPPLEMENTARY NOTES

12a. DISTRIBUTION/AVAILABILITY STATEMENT

Unrestricted

Approved for public release; distribution unlimited.

12b. DISTRIBUTION CODE

13. ABSTRACT *(Maximum 200 words)*

During the four months this grant was operative, a paper expanding on the Arecibo Initiative in Dynamics of the Atmosphere (AIDA '89) incoherent scatter/imaging Doppler interferometry (ISR/IDI) radar comparisons, which used revised data from both techniques, was prepared, and has subsequently been submitted and accepted for publication in the Journal of Atmospheric and Terrestrial Physics. In this paper, "Mesospheric Wind Studies During AIDA Act '89: Morphology and Comparison of Various Techniques," by R. S. Turek, K. L. Miller, R. G. Roper and J. W. Brosnahan, all of the measured line of sight velocity profiles for which data was available from both techniques, rather than a few selected profiles as previously analyzed, were subjected to a statistical analysis. This resulted in comparison of over 200 profiles, ten times more than the 20 previously published. After establishing that the sum of the prevailing wind, diurnal and semidiurnal tides deduced from the IDI data represented the statistical mean of the ISR data, we determined the morphology of the prevailing winds and tides over Arecibo during the April and May AIDA campaigns. The results are presented in this report.

14. SUBJECT TERMS	15. NUMBER OF PAGES 41
	16. PRICE CODE

17. SECURITY CLASSIFICATION OF REPORT	18. SECURITY CLASSIFICATION OF THIS PAGE	19. SECURITY CLASSIFICATION OF ABSTRACT	20. LIMITATION OF ABSTRACT
Unclassified	Unclassified	Unclassified	

Analysis of Mesospheric Winds and Waves

ABSTRACT

During the four months this grant was operative, a paper expanding on the Arecibo Initiative in Dynamics of the Atmosphere (AIDA '89) incoherent scatter/imaging Doppler interferometry (ISR/IDI) radar comparisons, which used revised data from both techniques, was prepared, and has subsequently been submitted and accepted for publication in the Journal of Atmospheric and Terrestrial Physics. In this paper, "Mesospheric Wind Studies During AIDA Act '89: Morphology and Comparison of Various Techniques," by R. S. Turek, K. L. Miller, R. G. Roper and J. W. Brosnahan, all of the measured line of sight velocity profiles for which data was available from both techniques, rather than a few selected profiles as previously analyzed, were subjected to a statistical analysis. This resulted in comparison of over 200 profiles, ten times more than the 20 previously published. After establishing that the sum of the prevailing wind, diurnal and semidiurnal tides deduced from the IDI data represented the statistical mean of the ISR data, we determined the morphology of the prevailing winds and tides over Arecibo during the April and May AIDA campaigns. The results are presented in this report.

STUDENTS GRADUATED UNDER THIS CONTRACT

No students graduated during the four-month period of this contract.

PUBLICATIONS THIS CONTRACT PERIOD

None

Analysis of Mesospheric Winds and Waves

What follows on the subsequent pages of this report are the text and figures of the paper "Mesospheric Wind Studies During AIDA Act '89: Morphology and Comparison of Various Techniques," by R. S. Turek, K. L. Miller, R. G. Roper and J. W. Brosnahan, as accepted for publication in the Journal of Atmospheric and Terrestrial Physics.

"Mesospheric Wind Studies During AIDA Act '89. Morphology and Comparison of Various Techniques"

R. S. Turek[+] and K. L. Miller,

(both at the Center for Atmospheric and Space Sciences

Utah State University

Logan, Utah 84322-4405)

R. G. Roper (School of Earth and Atmospheric Sciences

Georgia Institute of Technology

Atlanta, Georgia, 30332-0340)

and

J. W. Brosnahan (LaSalle Research Corporation

LaSalle, Colorado, 80645)

Abstract - The Arecibo Initiative in Dynamics of the Atmosphere (AIDA) '89 was a multi-instrument campaign designed to compare various mesospheric wind measurement techniques. Our emphasis here is the comparison of the incoherent scatter radar (ISR) measurements with those of a 3.175 MHz radar operating as an imaging Doppler interferometer (IDI). We have performed further analyses in order to justify the interpretation of the long term IDI measurements in terms of prevailing winds and tides. Initial comparison of 14 profiles by Hines et al., [1993] showed good agreement between the ISR and IDI measurements up to about 80 km, with fair to poor agreement above that altitude. We have compiled statistics from 208 profiles which show that the prevailing wind and diurnal and semidiurnal tides deduced from the IDI data provide a background wind about which both the IDI and ISR winds are normally distributed over the height range from 70 to 97km. The 3.175 Mhz radar data have also been processed using an interferometry (INT) technique [Van Baelen and Richmond, 1991] and two spaced antenna (SA) techniques [Meek, 1980; Briggs, 1984] to determine the three-dimensional wind vector. These are then compared with the IDI results. Tidal amplitudes and phases were calculated using the generalized analysis of

[+] Now at Department of Physics
U.S. Air Force Academy
Colorado Springs, CO 80840-6254

Groves [1959], historically used on meteor wind radar data. Results show a predominance of the diurnal S_1^1 tidal mode in the altitude range 70-110 km, reaching a maximum amplitude 45 m/s at 95 km, with semidiurnal amplitudes being about 10-15 m/s throughout the height range considered. There is evidence of the two day wave in data from 86-120 km, with amplitudes on the order of 20 m/s.

Introduction

The AIDA '89 campaign was in part designed to provide the framework for multi-instrument radar observations of the middle atmosphere. One of the fundamental objectives of AIDA '89 was to test the validity of the MF/HF "partial reflection" measurement of atmospheric 'drifts,' following a suggestion by Hines and Rao [1968] that the presence of gravity wave perturbations of the background electron density could contaminate MF/HF radar wind measurements. The experimental set-up involved the use of the Arecibo 430 Mhz incoherent scatter radar (ISR) facility, the MAPSTAR Imaging Doppler Interferometer (IDI), operating at a frequency of 3.175 Mhz, a 50 Mhz meteor wind radar, and a medium frequency spaced-antenna radar system. Detailed discussions of the individual systems and the overall experimental configuration are given in the recent literature [Journal of Atmospheric and Terrestrial Physics Special Issue, March 1993].

The data used in our study were collected during the second and third intervals of the AIDA 89 campaign, referred to as Scene II (28 March - 11 April 1989) and Scene III (02 May - 09 May 1989). Initial comparisons of the Incoherent Scatter (ISR) - Imaging Doppler Interferometer (IDI) data as published in the Special Issue showed agreement between the 'winds' measured by these techniques only up to 80km, with discrepancies often as large as 40m/s (maximum 80m/s) up to 97km, the maximum usable height for D region ISR wind determinations. Because both the ISR and IDI data have undergone some modification in the more rigorous reduction procedures used in recent re-analyses, updated plots of the previously published comparisons of ISR - IDI - Meteor Wind Radar (MWR) profiles [Hines et al., 1993] are presented. Due to the lack of data available from the Arecibo spaced-antenna system, our quantitative study is restricted to comparisons between data obtained from the ISR and MAPSTAR radars (the output of each MAPSTAR radar receiver was individually recorded so that not only IDI but also spaced antenna analyses could be applied). We first perform a comparison between line-of-sight drift velocities obtained from the different techniques, rather than assuming zero vertical wind and projecting the results into the horizontal, as was done in Hines et al [1993]. We have used this approach since the direct line of sight ISR measurement contains the vertical velocity component, and the IDI technique calculates the three dimensional wind vector, which can then be projected onto the ISR line of sight direction. As

stated by Hines et al. [1993], "The basic and unequivocal measurement is of the velocity in the line of sight direction." We then apply the Groves [1959] tidal analysis to the IDI scattering point data and present the resulting mean winds and tidal amplitudes and phases.

Line-of-Sight Drift Comparisons

The primary atmospheric volume of interest for the AIDA radar study was the 70-100 km region over the Arecibo heater facility, where the MAPSTAR radar was located. The Arecibo ISR is located 17 km to the SSW of the heater facility; therefore, when the ISR beam was pointed at a zenith angle of 11.3° and in an azimuthal direction of 33°, its line-of-sight intersected the MAPSTAR main beam at an altitude of 85 km, the center of the volume of interest. We then performed a comparison between the ISR line-of-sight velocity and the projection of the IDI three-dimensional motion vectors on the ISR beam direction:

$$V(IDI) = u \sin(11.3)\sin(33) + v \sin(11.3)\cos(33) + w \cos(11.3) \quad (1)$$

where u, v, and w are the zonal, meridional, and vertical components of the motion determined by the IDI method. The IDI method identifies scattering regions or "points" based on Fourier transformed phase consistency across a multiple-receiver array. A number of scattering point parameters are determined, including radial velocity, three-dimensional location, and the amplitude, phase and polarization of the returned signal. Detailed descriptions of the IDI scattering point analysis method and the subsequent determination of the three-dimensional wind vector are given in the literature [Adams et al., 1985; 1986, Brosnahan and Adams, 1993] and will not be presented here. However, one should note that the IDI line of sight velocity is calculated from a three dimensional vector averaged over a horizontal slab some 40 to 50km in diameter (the slab diameter increasing with height because of finite beam width), while the ISR line of sight is still within the near field of the Arecibo dish, and is thus a pencil beam 300m in diameter throughout the height range.

ISR line-of-sight velocities with 600 m resolution were obtained by using the pulse-to-pulse technique involving a 13 baud, 4 msec Barker code - the method described in detail by Mathews [1976] and Harper [1978]. Due to the broadening of the backscattered ISR spectrum with increasing altitude, this technique is generally limited to a maximum altitude of around 95-100 km. The minimum altitude where useful measurements are observed is determined by the power of the backscattered signal, and is typically 65-70 km during daylight hours. In this study the ISR data were restricted to the 70-97 km altitude range, with the spectra averaged over 3 km height intervals at 600 m increments. The data were then spline-interpolated to give

values at one kilometer intervals. The spectra were also temporally averaged over intervals on the order of 25 minutes each.

IDI line-of-sight velocity values were computed based on scattering points observed in 3 km altitude bins, 1.5 km above and below the given altitude. For example, the velocity values computed at 90 km were obtained by using all scattering points from 88.5 km to 91.5 km. This procedure was used from 70 to 97 km (the ISR altitude range) in 1 km steps. Error bars for both the IDI and ISR line-of-sight velocities were also computed; velocities for which either the IDI or ISR error was larger than 3 m/s (translating to a horizontal velocity error of 15 m/s if vertical motion is negligible) were considered unreliable and not considered in the comparison. This same rejection criterion was used in selecting the Hines et al., [1993] data; however, a limit equivalent to 2 m/s (a horizontal velocity error of 10 m/s for zero vertical velocity.), was used as the "goodness of fit" criterion, with disparities between IDI and ISR winds larger than this being deemed unacceptable. With only a 25 minute sampling interval (as opposed to the one to two hours of the Hines et al. [1993] comparison), our IDI data base suffers from having, at times, a marginal number of scattering points contributing to the wind calculation. This fact is not always evident in the in the error estimates as currently calculated (see Brosnahan and Adams, 1993), and gives rise to profile outliers. We are investigating alternate means of error calculation.

The MAPSTAR radar data were recorded in raw time-domain format (complex voltages as a function of time), allowing the same data to be processed using other MF/HF radar wind methodologies. In this study, we applied three different analysis methods to the raw MAPSTAR data. Two of these techniques involve the application of the spaced-antenna Full Correlation Analysis (FCA), with somewhat different acceptance/rejection criteria. The first method is the one in use at the University of Saskatoon [Meek, 1978; 1980] and referred to here as the SAS (Spaced-Antenna, Saskatoon) routine. The second SA techniques is the one in use at the University of Adelaide, and referred to here as the SAA (Spaced-Antenna, Adelaide) method. One should note that the acceptance criteria employed in the application of both these methods is that devised for the Arecibo Observatory MF radar, which are closer to those of the SAA rather than the SAS method. Finally, we applied a relatively new, three-dimensional, non-imaging radar interferometry method developed by Van Baelen and Richmond [1991], and referred to here as the INT (interferometry) technique. A three-dimensional drift vector is determined with each of these three methods at 3 km altitude steps from 60-120 km. The appropriate line-of-sight velocity is then computed from Equation (1) in the same manner as for the IDI method.

The details of the 50MHz VHF meteor radar used in comparisons between the IDI, ISR and MWR techniques have been described by Djuth and Elder [1993].

In an earlier comparison between IDI and ISR velocities conducted by Hines et al. [1993], both velocities were projected onto the horizontal plane, with the assumption of zero vertical velocity. The results were shown pictorially, but, while an explanation of the discrepancies was given in terms of Doppler scavenging by internal atmospheric gravity waves, quantitative comparison was made for less than 20 profiles. In all of our comparisons, as mentioned above, the vertical velocity is included, and we make an attempt to quantify the overall agreement in the line of sight components of over 200 profiles. Our study also involves shorter temporal intervals (25 min. as opposed to 1-2 hr), which should mitigate possible discrepancies observed between the two techniques due to the temporal variation of the wind field itself. We should point out here that the data from both the ISR and IDI radars have been extensively re-analysed in order to assure the maximum data quality. In general, this has resulted in the rejection of some previously accepted data and very minor changes in most of the rest, with up to 10 m/s change in the line of sight in only a few of the acceptable profiles. The extent of these changes is illustrated by the plots of Figure 1, (which are the line of sight equivalents of the previously published Figure 5 in Hines et al., [1993], to which they can be directly compared by multiplying the Hines et al. horizontal velocities by sin 11.3 = 0.2). In contrast to the original profiles, the IDI results are closer to the MWR in all but the 1217hrs - 1359hrs April 10 period. To some extent this may be fortuitous, in that the meteor radar line of sight is at a zenith angle of 37°, rather than 11.5° (Djuth and Elder, 1993).

In the quantitative comparisons in the present paper, line of sight velocities at each altitude for which both the IDI and ISR individual line of sight velocity measurement uncertainties are $\leq$ 3 m/s are compared and the difference between the two values, DV, is determined. We then compute the mean difference DV over all altitudes for which we have good IDI and ISR data, the number of altitudes being $\leq$ 28. Figures 2, 3, and 4 show several comparison intervals that fall into the DV $\leq$ 3m/s, 3m/s < DV $\leq$ 6 m/s, and DV > 6 m/s categories, respectively. Note that, as can be seen from Figure 3, most of the $\leq$ 6 m/s comparisons satisfy our criterion for $\leq$ 3 m/s agreement below 90km.

If we now examine the IDI/ISR discrepancies for all the comparison intervals at each height for Scene II (28 March - 11 April, 1989) and Scene III (02 May - 09 MAY, 1989), we obtain the distributions shown in Figure 5. From the 2717 comparisons (from the 137 profiles) made during Scene II, we have 1574 exhibiting agreement to better than 3 m/s (57.9%), 753 with agreement between 3 and 6 m/s (27.7%) and 390 for which the disparity is > 6m/s (11.1%). The Scene III comparison is even more encouraging: from 1337 total comparisons, we obtain 834 (62.4%), 386 (28.9%) and 117 (8.7%) comparisons for each of the respective categories. In addition the Scene II IDI/ISR line of sight velocity deviations have a mean of 0.09 m/s, with a standard deviation 4.08 m/s (mean absolute difference of 3.14 m/s); Scene III

deviations have a mean of 0.12 m/s, with a standard deviation of 3.57 m/s (mean absolute difference of 2.75 m/s). In other words, as can be seen from figure 5, the observed velocity deviations are normally distributed about a mean very near to zero.

We now further examine the ISR and IDI comparison, with the hope of explaining, at least to some degree, the intervals for which there exists poor agreement. Since the intervals are of finite duration, there certainly exists the possibility that the actual wind variability over the duration of the interval might influence the comparison statistics. If, for instance, the IDI analysis yielded more scattering points at the beginning of a given interval, the subsequent velocity measurements obtained might be different from an ISR measurement that might be weighted toward a later time in the interval. To obtain an approximate measure of the variability of the data over the time scale of these intervals (25 min.), we compared the IDI and ISR data interval-to-interval differences for consecutive intervals. In other words, if two intervals were consecutive in time (one following immediately after another), we compared the difference between the IDI data from the two intervals, and then performed the same comparison with the ISR data. This then gives us a feel for the difference in the line-of-sight velocity between identical measurement methods, and therefore presumably relates to the physical difference in the motion itself over the time scale involved.

Of the 137 intervals used during Scene II, 89 were consecutive in time, while 43 of the 71 Scene III intervals were consecutive in time. Given two consecutive intervals, we then examine velocity differences in the following manner:

1) Compute the mean difference in the IDI values between the two intervals.

2) Compute the mean difference in the ISR values between the two intervals.

3) Compare the IDI/ISR mean differences of both the first and second intervals, separately, to the values found in 1) and 2) above.

The results of this comparison for Scene II and Scene III are shown in Figure 6.

Several characteristics of this data are evident in Figure 6. First, while there is considerable scatter in the data, they appear to be normally distributed - for most of the comparisons there is little difference between the IDI and ISR results. We note with some surprise, however, that while both large IDI/ISR discrepancies and large variations from one interval to the next in both the IDI and ISR data exist, they are apparently uncorrelated; there appears to be little tendency for the scattered points to congregate along the diagonal. We had anticipated otherwise, in that we had hypothesised that, since both the IDI and ISR techniques do not, in fact, produce a continuous data stream with time, the possibility that one technique measured data perhaps early in the interval, and the other perhaps later, with the wind itself being variable on even the shorter timescale intervals involved here, could account for a considerable portion of the variance. Finally, we see that the Scene III data exhibits more

scatter, but has fewer large discrepancy intervals than that observed in Scene II. This tends to be true for both the IDI data and the ISR data.

As a final comparison of the IDI/ISR data, we look at the velocity discrepancies as a function of altitude. The earlier work by Hines et al. [1993], showed fairly good agreement between the IDI and ISR results below 80 km, with much poorer agreement at higher altitudes. The results of our study indeed show good agreement below 80 km, but also show fairly good agreement to much greater altitudes, bearing in mind that we are unable, because of the shorter comparison intervals involved, to employ as stringent a criterion for agreement as Hines et al. [1993]. Our criterion for excellence here is based on the standard for agreement established by the 70 to 80 km differences, which both we, and Hines et al. [1993], deem satisfactory. The mean discrepancies as a function of height, averaged over all intervals for Scene II and Scene III, are shown in Figure 7. The Scene II data shows excellent agreement below 83 km, then fairly good agreement to about 94 km, with increasingly poor agreement above that height. The data for Scene III are characterized by very good to excellent agreement up to 95 km, with somewhat poorer agreement above. In addition, the Scene III data are characterized by a curious 'hump' in the 79-83 km range, a feature not seen in the Scene II data. However, aside from the 'hump', the agreement in Scene III is somewhat better than in Scene II.

In summary, the comparison between the IDI projected line-of-sight data and the ISR observed line-of-sight data are better than that described by Hines et al. [1993], although it could be argued that, because of the measurement error limitations inherent in the comparison of shorter data intervals, all we have done is increase the bounds, thereby appearing to make the comparisons better. In answer to this possible criticism, we would ask the reader to consider the bounds of the 70 to 80 km results, where there is no contention, and to relate those to the differences at higher altitudes. Considering the limitations of this type of comparison, i.e., utilizing dramatically different beam widths (700 m vs. ~ 50 km) we believe the agreement is quite encouraging. We do observe greater discrepancies above 92-95 km, but this is also the altitude region where the ISR backscatter spectrum undergoes significant broadening and is therefore less conducive to velocity calculations from the pulse-to-pulse method. In addition, our results show an overall comparison that is certainly as good as earlier comparisons of the Arecibo ISR with meteor wind results [Mathews et al., 1981].

We now compare the IDI line-of-sight velocities with those determined from the analysis of the raw time series by the INT, SAS, and SAA techniques. Due to convenience in later tidal analysis, the comparison intervals for this study were one hour in length centered about each hour in local mean solar time (LMST = UT - 4 hours 28 minutes). The IDI vs. INT, IDI vs. SAS, and IDI vs. SAA comparisons are shown in Figures 8-10, respectively. We see that for all three techniques, the agreement with IDI is good during nighttime hours (1800-0600 LMST)

and excellent during daytime hours (0700-1700 LMST). As in the IDI/ISR comparison, we note that the agreement is somewhat better during Scene III than Scene II. In general, the three techniques exhibit about the same agreement with the IDI results; however, there do exist variations in the relative agreement of the three methods between daytime and nighttime hours and between the two AIDA scenes. The reader should note that we have not attempted to optimize either the SAA or SAS techniques for the prevailing ionospheric conditions, and therefore any lack of agreement should not be interpreted as indicating either is "better" or "worse" than the other.

As we did in the IDI/ISR comparison, we again perform an analysis of the relative agreement of the three techniques vs. IDI as a function of altitude. To compare with the IDI/ISR daytime comparison shown earlier (Figure 7), we show the daytime comparisons for Scene II and Scene III in Figure 11. This figure shows that for all three methods, the average agreement with IDI is very good to at least 100 km, with slightly less agreement at higher heights. This could in fact be related to the fact that the INT, SAS, and SAA methods assume the altitude of the calculated motion is equal to the range, in other words, the average pattern is assumed to be overhead. In contrast, the altitudes of the scattering points identified by the IDI technique may be several km less than the range for larger zenith angles (up to 16° here). Therefore, we might expect deviations in the compared velocities due to differences in the actual heights of the observed motions. Since the actual distribution of scatterers includes points far removed from the zenith, we might expect the winds measured by the INT, SAS, and SAA techniques to be more appropriate to some altitude lower than that given by the range itself, or more likely, be a mixture of winds from different altitudes. However, the agreement between the IDI and the other three MF/HF radar techniques is still very encouraging.

By averaging data over each scene, we have determined that, while individual profiles may show significant lack of agreement (as detailed in Hines, 1993), the long term mean differences are of the order of the errors associated with the experimental determinations. Such agreement reinforces the assertion that the application of the Groves analysis to the IDI data, as previously performed by Roper et al. [1993], results in the determination of real tides. However, this evidence, even when coupled with the arguments presented by Roper et al. [1993], might still be considered circumstantial. We have, therefore, applied a further test which substantiates the reality of the tidal determinations. The ideal would be, of course, to apply the Groves analysis to the ISR data. This is not, however, possible, since the ISR data is available only for a few hours each side of noon. Therefore, we have taken the difference between the Groves analysis of the IDI results (projected on the ISR line of sight) and the velocities from the IDI and ISR measurements to characterize the relevancy of the Groves results to each data set. The results are shown in Figure 12. To produce this figure, we have

taken as a standard the line of sight profile representing the mean, diurnal and semidiurnal components resulting from applying the Groves analysis to the 24 hours of IDI data (from noon to noon) which includes the particular interval. From this profile we have subtracted values from the IDI and ISR profiles at 1km intervals within ± 4.5km of 75, 84 and 93km altitude. Figure 12 shows how well the line of sight wind vector resulting from applying the Groves analysis fits not only the IDI line of sight, *but also the ISR*. Values defining the Gaussian fits are listed in Table 1.

The fact that the Groves analysis fit to the IDI data produces a close to normal distribution at all altitudes is no surprise - after all , the Groves is a least squares fitting technique. The fact that the Groves produces almost identical fits to the ISR data (both mean difference and standard deviations within < 2.0m/s of each other for IDI and ISR data) is, it seems to us, the ultimate justification for the IDI technique measuring real winds, at least on a diurnal time scale. It is tempting to interpret the σ values of 3.0 to 6.1m/s as simply representing random winds with, for vertical wind zero, horizontal amplitudes at 33° azimuth of 15 to 30m/s, but this would leave no room for error, which we find to be of just these magnitudes! We note that the comparisons show greater variance for April 5 through 11 than for May 2 through 9, but this is no surprise, since the reason for choosing the April dates as the primary AIDA interval was the evidence (from nighttime optical measurements) of considerable short period wave activity during the first half of that period. There is no doubt that the random wave field must be a contributor to the variance observed. We also note that the Groves, while providing a mean to both the IDI and ISR results, about which both are apparenly normally distributed, yields an ISR variance above 80 km which is greater than that of the IDI.

Due to the encouraging results discussed in this section, it would appear that the IDI technique measures the bulk motion of the middle atmosphere, with, once again, the Roper et al. [1993] "on a diurnal timescale" caveat. We therefore submit the IDI data to tidal analysis to examine the tidal structure of the middle atmosphere over Arecibo. The results of this analysis are given in the following section.

Tidal Structure over Arecibo.

In this section we will discuss the use of the IDI data in determining the tidal structure of Arecibo during AIDA '89. The IDI scattering point data set lends itself well to tidal analysis via the method developed by Groves [1959], as previously discussed by Roper et al. [1993]. While the Groves analysis has historically been used in the determination of tidal winds from meteor wind data, we find that the great number of IDI scattering points observed (on the order of 100 greater than meteor echoes) allows greater spatial and temporal resolution in the

resultant wind. We note, however, (see Roper et al., 1993) that 10 times as many scattering points compared to meteor trails are needed in order for the Groves to perform a stable inversion - this fact needs further investigation).

In the work of Roper et al. [1993], tidal winds for the period 5-11 April 1989 were presented, which cover roughly the second half of Scene II. In this paper we present the mean wind, diurnal, and semidiurnal amplitudes and phases for both Scene II and Scene III of the AIDA campaign. In our application of the Groves analysis, we assume the measured background wind consists of a mean wind, a diurnal, and a semidiurnal tidal component. In addition, we allow a seventh order polynomial variation of the zonal and meridional wind with height, and a fifth order variation of the vertical wind; two orders greater than that performed by Roper et al. [1993]. Due to increased computational power available, we were also able to process all scattering points with zenith angles between 3° and 16°. This allowed an order-of-magnitude increase in the number of scattering points involved in the calculation, with presumably superior results.

The overall (mean wind plus tides) zonal and meridional components determined from the Groves analysis are shown as contour plots in Figure 13. We note that the winds from the entire Scene II data look remarkably similar to those presented by Roper et al. [1993]. This leads us to two conclusions: 1) two somewhat different applications of the Groves analysis produce similar results, giving us confidence in the suitability of IDI data to the analysis, and 2) the tidal structure of the atmosphere is fairly stable over this six to fourteen day period.

The diurnal and semidiurnal amplitudes determined from the Scene II and Scene III data are depicted in Figure 14, with the associated phases given in Figure 15. It is apparent from these figures that for Scene II data, the diurnal tide is dominant over the altitude region from 70-100 km. The Scene II diurnal zonal and meridional phases are strikingly linear with height through most of the height range considered. The downward propagation of phase corresponds to an upward propagation of tidal energy, consistent with the theory that the oscillations result from energy introduced in the lower atmosphere [Hines, 1963; Forbes, 1982]. In addition, the phases are essentially in quadrature; the meridional leading the zonal by six hours ($\pm$1 hour) at most altitudes. The phase quadrature is consistent with a well-developed clockwise rotation, as is required for tidal motions in the northern hemisphere. A linear least-squares fit to the diurnal phases over the altitude range 72-106 km yields zonal and meridional vertical wavelengths of 28.3 and 27.7 km, respectively. This compares to vertical wavelengths of 29.1 and 28.2 km from the Forbes [1982] model. The diurnal vertical wavelengths observed during AIDA indicate the predominance of the S_1^1 mode, which is to be expected at lower latitudes [Chapman and Lindzen, 1970], and previously observed at Arecibo [Mathews, 1976]. The Scene II semidiurnal tide is somewhat less pronounced, with significant amplitudes only above 100 km.

where the zonal and meridional phases are essentially in quadrature. In this region, from 100-116 km, the vertical wavelengths are on the order of 100 km, which correspond to Hough modes associated with the S_2^2 semidiurnal tide.

The tidal structure observed during Scene III tends to be somewhat different from that of Scene II, with much larger semidiurnal amplitudes in Scene III. The diurnal tidal phase for both zonal and meridional components show a near-linear phase relationship with height below 90 km, with the expected downward phase propagation. The vertical wavelengths of the Scene III diurnal zonal and meridional tidal winds are also somewhat smaller than in Scene II, being 23.9 and 23.8, respectively. Above 90 km, the phase structure becomes very interesting; the meridional phase continues on in a linear fashion, while the zonal phase shows an abrupt change and exhibits a slight upward propagation of phase. The Scene III semidiurnal tide is much more pronounced than in Scene II, with average amplitudes on the order of 50% greater. While the phase pattern is not altogether linear with height, it is approximately in quadrature, and indicates downward propagation of phase and a long vertical wavelength as found in Scene II.

In addition to using the Groves analysis on IDI scattering point data, we also calculated tidal parameters from the hourly wind values obtained from the IDI, INT, SAS, and SAA MF/HF radar methods. As in the Groves analysis, we analyzed these hourly wind data to determine the mean wind, the diurnal, and the semidiurnal tidal components. A comparison of the mean (the sum of the prevailing, diurnal and semidiurnal) winds observed by the various methods during Scene II and Scene III is given in Figure 16. We see that the mean winds determined from the various methods are quite similar. Furthermore, as an example of the comparison of the overall wind (prevailing plus diurnal plus semidiurnal), a contour plot of the Scene II zonal wind from the IDI, INT, SAS, and SAA hourly mean data is shown in Figure 17. While there appear to be some differences, it should be remembered that small changes in velocity can cause what appear to be significant changes in the contour lines. Overall, the agreement is quite good, with the wind at most altitudes and times differing by less than 10 m/s. These comparisons show that, at least in the determination of tidal parameters, the various MF/HF radar techniques do yield similar results.

As a final note in the discussion of tidal behavior, we present the results of a periodogram analysis of the hourly wind data. The periodogram analysis calculates the spectrum of wind energy, defined as the sum of squares of the zonal, meridional, and vertical components of the wind, in discrete frequencies from 0.05 to 12 cycles per day. The wind energy for Scene II, as a function of altitude, is shown for the 48, 24, 12, 8, and 6 hr components in Figure 18. Again we note the dominance of the diurnal tide, with a peak amplitude of about 45 m/s at 94 km. The semidiurnal tide is on the order of 5-10 m/s below 100 km, and approaches 15-20 m/s at

higher altitudes. In addition, we note the presence of the two-day wave at altitudes from 85-120, with a peak amplitude of about 20 m/s at 90-95 km. Finally, we note that the amplitudes of the 8 and 6 hr components are insignificant at all altitudes from 60-120 km.

Conclusions

We have compared the ISR and IDI line-of-sight velocities for a large number of intervals during the AIDA '89 campaign. While some discrepancies are observed, the long term statistical comparisons using 100 or more profiles are more favourable than those made by Hines et al. [1993], who used only 20 profiles. In addition, the application of several MF/HF radar wind measuring techniques to the raw MAPSTAR radar data produce results that also compare well with the IDI results. We have also performed an extensive tidal analysis on hourly wind data produced by the IDI, INT, SAS, and SAA techniques. The mean winds and tidal structure determined from these various methods compare quite well and show the dominance of the diurnal tide in the March-April data, with a more significant semidiurnal tide in the May data. Both data sets show the semidiurnal tide to become increasingly important at higher altitudes, as has been previously observed at Arecibo [Harper, 1977; Mathews and Bekeny, 1979]. We have also applied the Groves [1959] analysis to the IDI scattering point data set. We note that in the Scene II data, where discrepancies between the IDI and ISR measurements are greater, the inferred diurnal tidal phases agree well with the theoretical predictions of Chapman and Lindzen [1970]; this would seem to be too much of a coincidence to have resulted from the imprinting from below of gravity waves producing tide-like oscillations in the sampled region.We conclude that the winds measured by the IDI and the other MF/HF radar methods are indeed compatible with those from the ISR over the long term. In addition, it would certainly appear from the comparisons presented here that the wind information extracted from the MF/HF radar measurements represent planetary wave and atmospheric tidal motion. There are often significant differences between the 25 minute IDI and ISR profiles, which may be explained by the inhomogeneity of the wind field within the viewing area at any given altitude [Kudeki et al. 1993], by the preferential detection by the MF/HF radar techniques of specular reflection by interfering wave fronts [Hines et al. 1993], by the more recent suggestion by Hines [1993], based on arguments presented in Hines [1991], that the strongest partial reflection returns come from the atmospheric equivalent of turbulent 'whitecaps' whose velocity contains components not only of the bulk motion, but also of the wave spectrum whose mutual interaction caused momentary, isolated wave breaking, by a combination of each of the above, or for some other as yet unsuspected reason. The question of

the relationship between the various interferometric velocities and SAD "true" and "apparent" velocities also requires further elaboration. However, it is our contention that the MF/HF radar planetary wave and tidal data compiled over the past three decades represent a useful climatology, and should be recognized as such.

Readers may perhaps criticize us for not referring to the wealth of data that has been accumulated over the years which has shown the consistency of, for example, meteor and MF/HF radar climatologies, such as those contained in the 1986 COSPAR International Reference Atmosphere [1990]. The purpose of this paper is not to write an overview (review) of the histories of the various upper atmosphere radar wind measuring techniques, but, rather, to address the specifics of the comparisons performed during the AIDA'89 campaigns, as these apply to the determination of planetary waves and tidal winds. We have mentioned the names of some of the major players in such endeavors - interested readers can follow up on these players if they so desire. We trust that those whom we have not mentioned will not feel slighted.

Acknowledgements

This research has been supported by the U.S. Air Force Office of Scientific Research under contracts F49620-J-93-0193 and F49620-93-1-0460, and the National Science Foundation under Grant # ATM-9216653. We acknowledge the contributions of the late Dr. Gene Adams, without whose scientific acumen, insight and perserverance there would be no IDI technique. We are indebted to Dr. C.O. Hines for identifying a problem associated with our initial interpretation of Figure 6, and to Dr. Michael P. Sulzer, of the Arecibo Observatory, for providing us with the ISR data. The Arecibo Observatory is operated by Cornell University under National Science Foundation sponsorship.

References

Adams, G. W., D. P. Edwards, and J. W. Brosnahan. 1985. The imaging Doppler interferometer: Data analysis. Radio Sci., 20(6), 1481-1492

Adams, G. W., J. W. Brosnahan, D. C. Walden, and S. F. Nerney. 1986. Mesospheric observations using a 2.66-Mhz radar as an imaging Doppler interferometer: Description and first results, J. Geophys. Res., 91(A2), 1671-1684

Briggs, B. H., 1984. The analysis of spaced sensor records by correlation techniques. MAP Handbook. 13, 166-186

Brosnahan, J. W., and G. W. Adams. 1993. The MAPSTAR imaging Doppler interferometer (IDI) radar description and first results, J. Atmos. Terr. Phys., 55(3), 203-228

Chapman, S., and R. S. Lindzen, 1970. *Atmospheric Tides*, Gordon and Breach Science Publishers, Inc., New York, 200 pp.

COSPAR. 1990. The COSPAR International Reference Atmosphere (CIRA '86); Part II, Adv. Space Res., 10(12), 267-315

Djuth, F.T., and J.H. Elder. 1993. The VHF radar system used during the Arecibo Initiative in Dynamics of the Atmosphere (AIDA) campaign '89, J. Atmos. Terrest. Phys., 55, 229-238

Forbes, J. M. 1982. Atmospheric Tides, 1, Model description and results for the solar diurnal component, J. Geophys. Res., 87(A7), 5222-5240

Groves, G. V.	1959	A theory for determining upper atmosphere winds from radio observations on meteor trails, J. Atmos. Terr. Phys., 16, 344-356
Harper, R. M.	1977	Tidal winds in the 100- to 200-km region at Arecibo, J. Geophys. Res., 82, 3243-3250
Harper, R. M.	1978	Preliminary measurements of the ion component of the incoherent scatter spectrum in the 60-90 km region over Arecibo, J. Geophys. Res. Lett., 5, 784-786
Hines, C. O.	1963	The upper atmosphere in motion. Quart. J. Roy. Met. Soc., 89, 1-41
Hines, C.O.	1991	The saturation of gravity waves in the middle atmosphere, Part I: critique of linear-instability theory, J. Atmos. Sci., 48, 1348-1359
Hines, C. O., G. W. Adams, J. W. Brosnahan, F. T. Djuth, M. P. Sulzer, C. A. Tepley and J. S. Van Baelen	1993	Multi-instrument observations of mesospheric motions over Arecibo: comparisons and interpretations, J. Atmos. Terrest. Phys., 55(3), 241-288
Hines, C.O., and R. Rhagava Rao	1968	Validity of three station methods of determining ionospheric motions, J. Atmos. Terrest. Phys., 30, 979-993
Kudeki, Erhan, Prabhat K. Rastogi and Fahri Surucu,	1993	Systematic errors in radar wind estimation: implications for comparative measurements, Radio Sci., 28(2),169-179

Mathews, J. D.	1976	Measurements of the diurnal tides in the 80- to 100-km altitude range at Arecibo, J. Geophys. Res., 81(25), 4671-4677
Mathews, J. D., and F. S. Bekeny	1979	Upper atmosphere tides and the vertical motion of ionospheric sporadic layers at Arecibo, J. Geophys. Res., 84(A6), 2743-2750
Mathews, J. D., M. P. Sulzer, C. A. Tepley, R. Bernard, J. L. Fellous, M. Glass, M. Massebeuf, S. Ganguly, R. M. Harper, R. A. Behnke, and J. C. G. Walker.	1981	A comparison between Thomson scatter and meteor wind measurements in the 65- 105 km altitude region at Arecibo, Planet. Space Sci., 29, 341-348
Meek, C. E.	1980	An efficient method for analyzing ionospheric drifts data, J. Atmos. Terr. Phys., 42(9/10), 835-839
Roper, R.G., G.W. Adams and J.W. Brosnahan	1993	Tidal winds at mesopause altitudes over Arecibo (18°N,67° W), April 5 - 11, 1989 (AIDA '89), J. Atmos. Terrest. Phys., 55,289-312
Van Baelen, J. S., and A. D. Richmond	1991	Radar interferometry technique: Three-dimensional wind measurement theory, Radio Sci., 26(5), 1209-1218

Reference is also made to the following publications:

Hines, C.O.	1993	AIDA'89 results and interpretations, Proceedings of the Workshop on Multiple Receiver Radar Techniques, August 1992, Urbana, Illinois, pp 47-48
Meek, C. E.	1978	The analysis of ionospheric drift measurements, ISAS Report, 127 pp., University of Saskatchewan, Saskatoon

Table 1

z (km)	mean (m/s)	σ (m/s)
Scene II, IDI		
93	0.5	4.2
84	-0.8	3.3
75	-0.4	3.0
ISR		
93	-0.4	6.1
84	-0.5	5.0
75	-0.3	3.5
Scene III, IDI		
93	-1.1	3.9
84	-0.4	3.5
75	0.5	3.6
ISR		
93	-1.7	4.9
84	-0.9	4.2
75	0.1	3.3

List of Illustrations.

Figure 9. As for Figure 8, except IDI/SAS (spaced antennae, Saskatoon) comparisons.

Figure 10. As for Figure 8, except IDI/SAA (spaced antennae, Adelaide) comparisons.

Figure 11. Mean line of sight velocity differences as a function of altitude for IDI/INT, IDI/SAS and IDI/SAA comparisons for
a)Scene II daytime data and
b) Scene III daytime data.

Figure 12 Plots of the distributions of IDI and ISR line of sight velocities about the Groves as a function of height (71 - 79, 80 - 88 and 89 - 97km) for April 5 - 11 and May 2 - 9, 1989. These plots are presented as justification for the discussion of the Groves results as tides.

Figure 13. Contour plots of winds determined by applying the Groves analysis to the IDI scattering point data, plotted as the sum of mean, 24 and 12 hour components:
a) zonal wind component for Scene II,
b) zonal wind component for Scene III,
c) meridional wind component for Scene II and
d) meridional wind component for Scene III.

Figure 14. Diurnal and semidiurnal tidal amplitudes determined from the Groves analysis of the IDI scattering point data:
a) zonal wind component for Scene II,
b) zonal wind component for scene III,
c) meridional wind component for Scene II and
d) meridional wind component for Scene III.

Figure 15. Diurnal and semidiurnal tidal phases determined from the Groves analysis of the IDI scattering point data:
a) diurnal phase for Scene II,
b) diurnal phase for Scene III,
c) semidiurnal phase for Scene II and
d) semidiurnal phase for Scene III.

Figure 16 Mean (prevailing) winds determined from the Groves analysis of the IDI data (labeled IDIG), and analysis of hourly mean IDI, INT, SAS and SAA "apparent" velocity data:

a) Scene II zonal,

b) Scene III zonal,

c) Scene II meridional and

d) Scene III meridional.

Figure 17. Contour plot of the zonal wind (the sum of the mean plus diurnal plus semidiurnal components) for Scene II, determined from the

a) IDI hourly wind data,

b) INT hourly wind data,

c) SAS hourly wind data and

d) SAA hourly wind data.

Figure 18. The variation with altitude of the wind energy per unit mass of the 48, 24, 12, 8 and 6 hour components determined from Scene II hourly wind data. The figures correspond to values obtained from the

a) IDI,

b) INT,

c) SAS and

d) SAA techniques.

Note the predominance of the diurnal wind at all altitudes from all techniques.

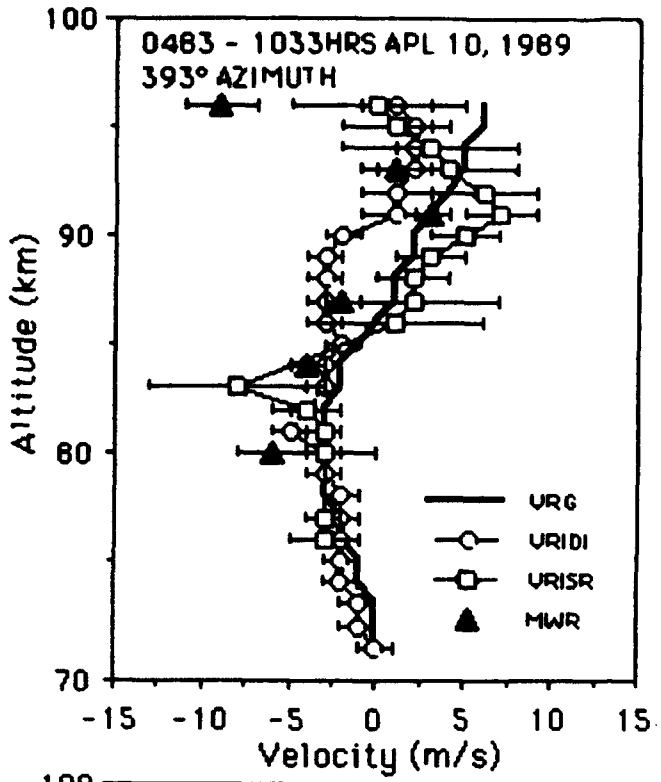
0483 - 1033HRS APL 10, 1989
393° AZIMUTH
URG
URIDI
URISR
MWR
Altitude (km)
Velocity (m/s)

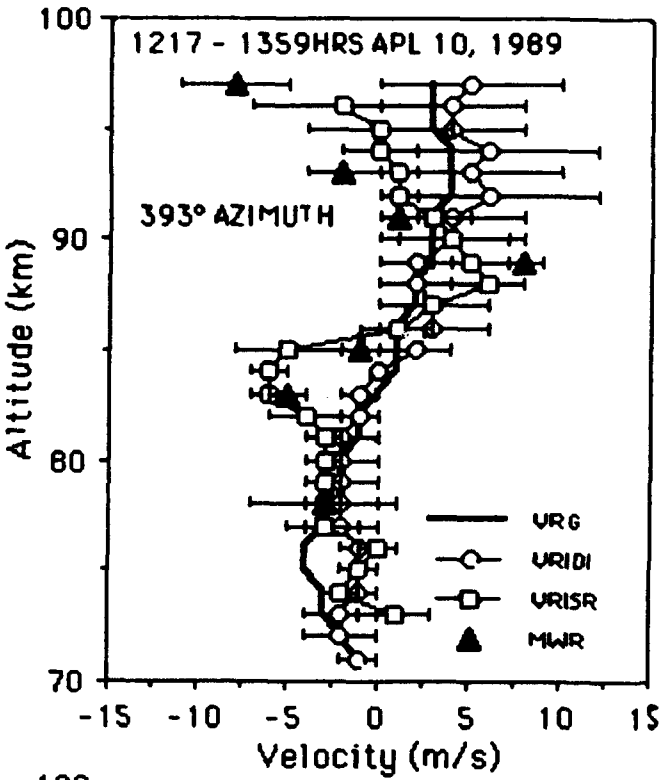
1217 - 1359HRS APL 10, 1989
393° AZIMUTH
URG
URIDI
URISR
MWR
Altitude (km)
Velocity (m/s)

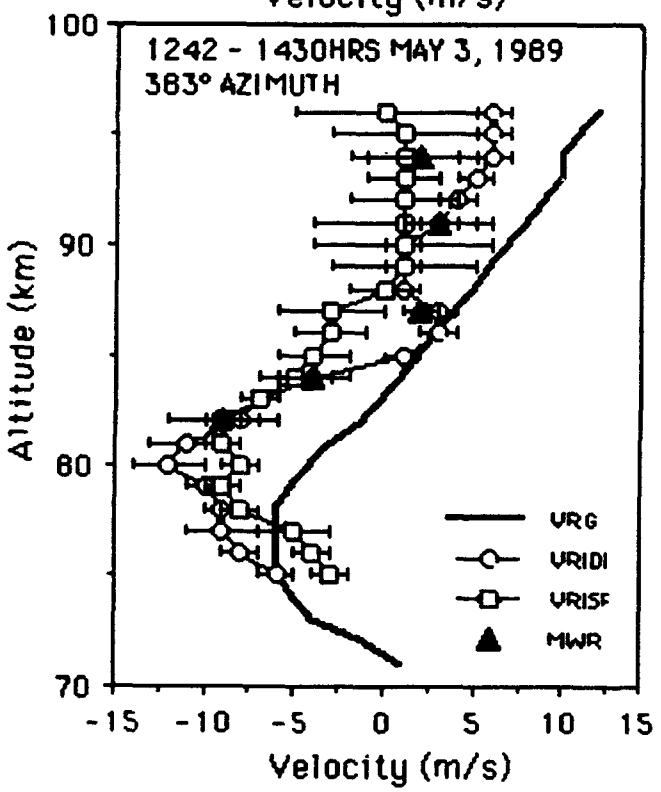
1242 - 1430HRS MAY 3, 1989
383° AZIMUTH
URG
URIDI
URISR
MWR
Altitude (km)
Velocity (m/s)

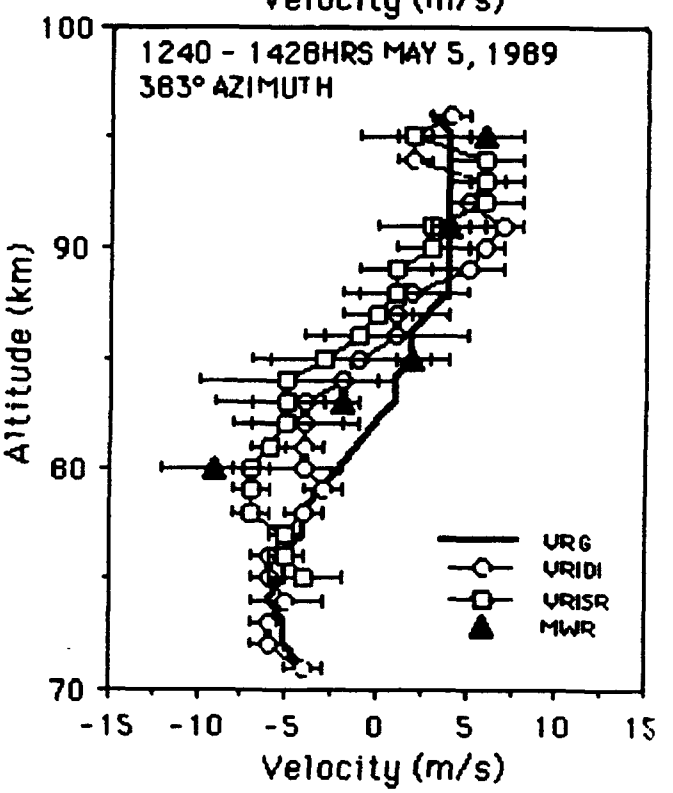
1240 - 1428HRS MAY 5, 1989
383° AZIMUTH
URG
URIDI
URISR
MWR
Altitude (km)
Velocity (m/s)

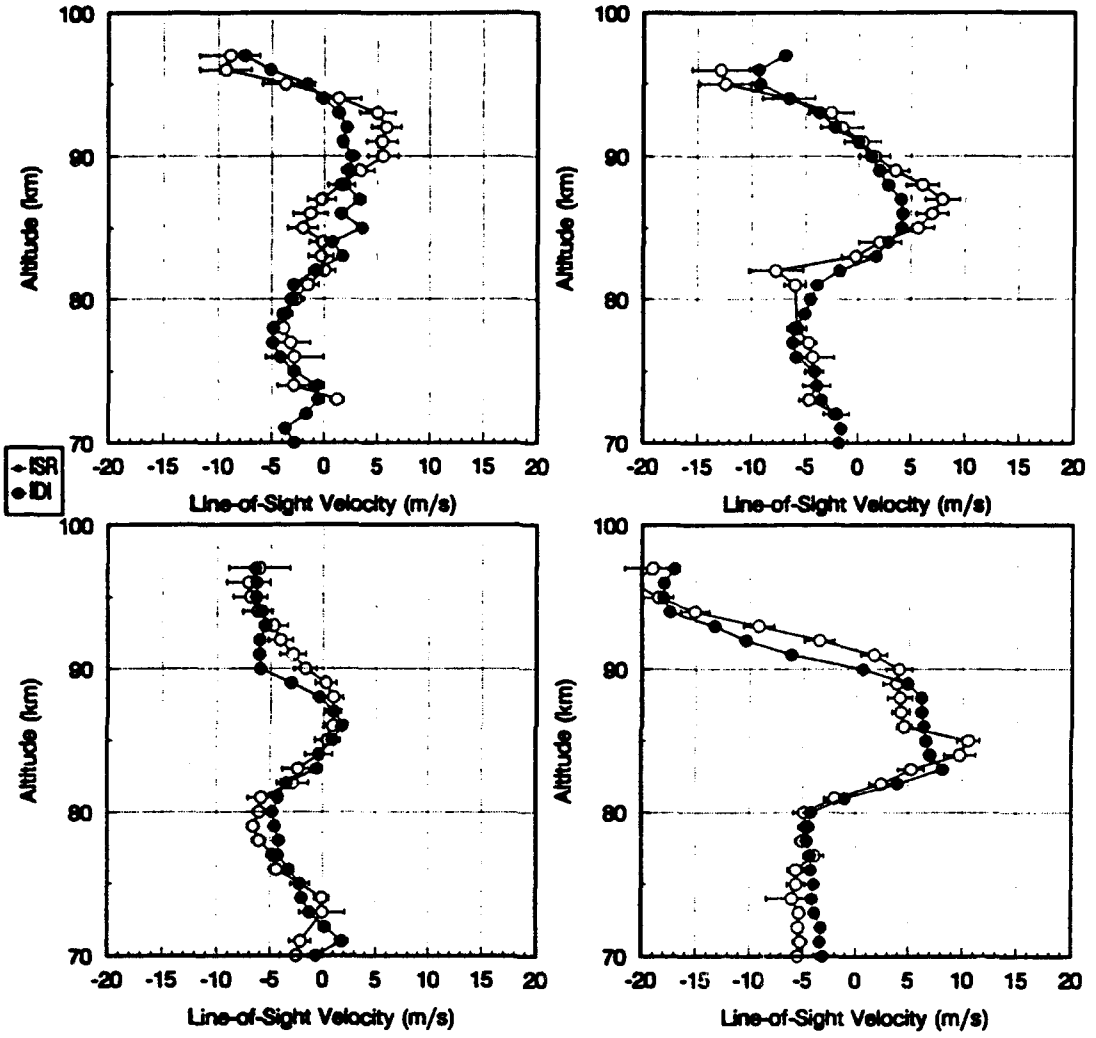
ISR
IDI
Altitude (km)
Line-of-Sight Velocity (m/s)
100
90
80
70
-20
-15
-10
-5
0
5
10
15
20

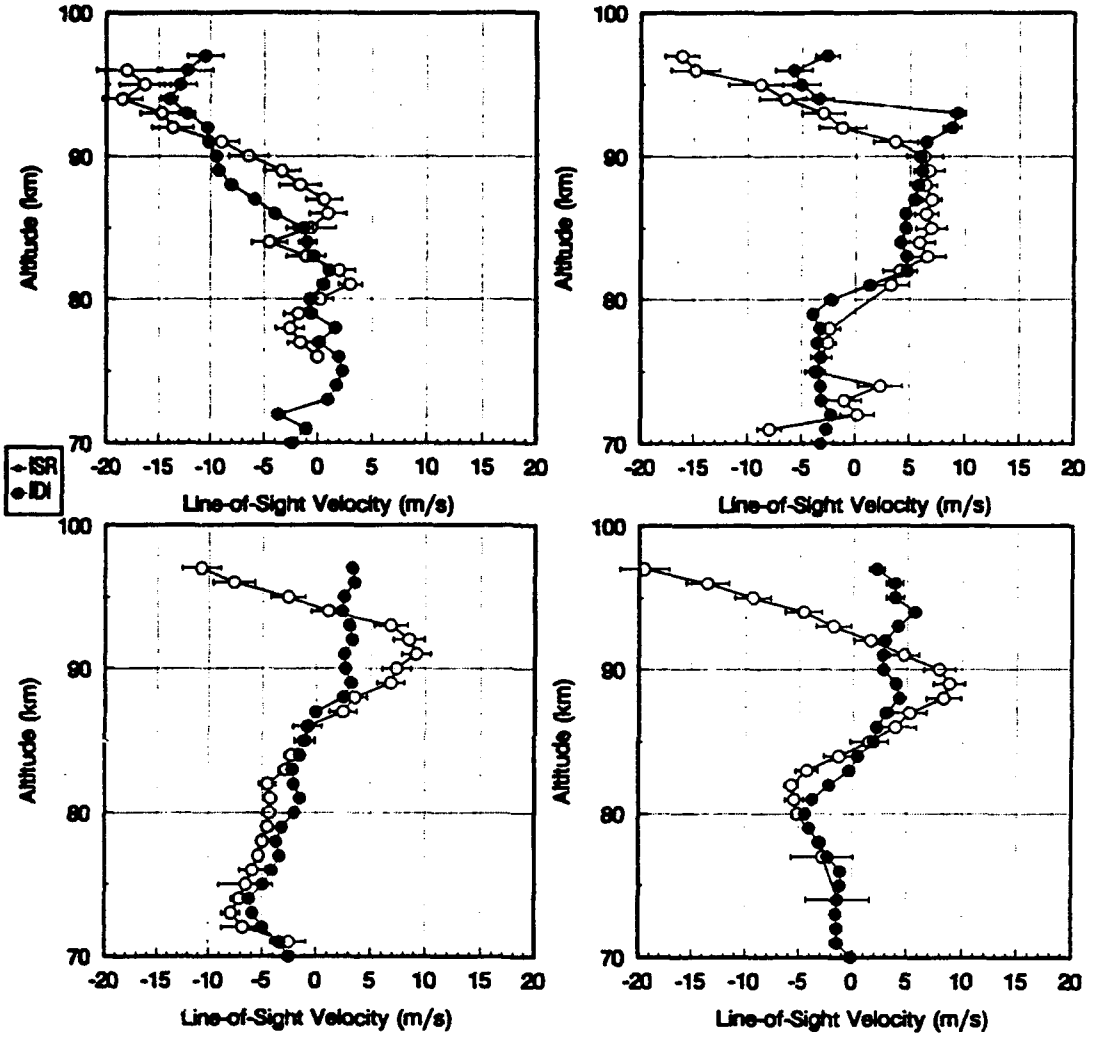
100
90
80
70
Altitude (km)
-20 -15 -10 -5 0 5 10 15 20
Line-of-Sight Velocity (m/s)
ISR
IDI

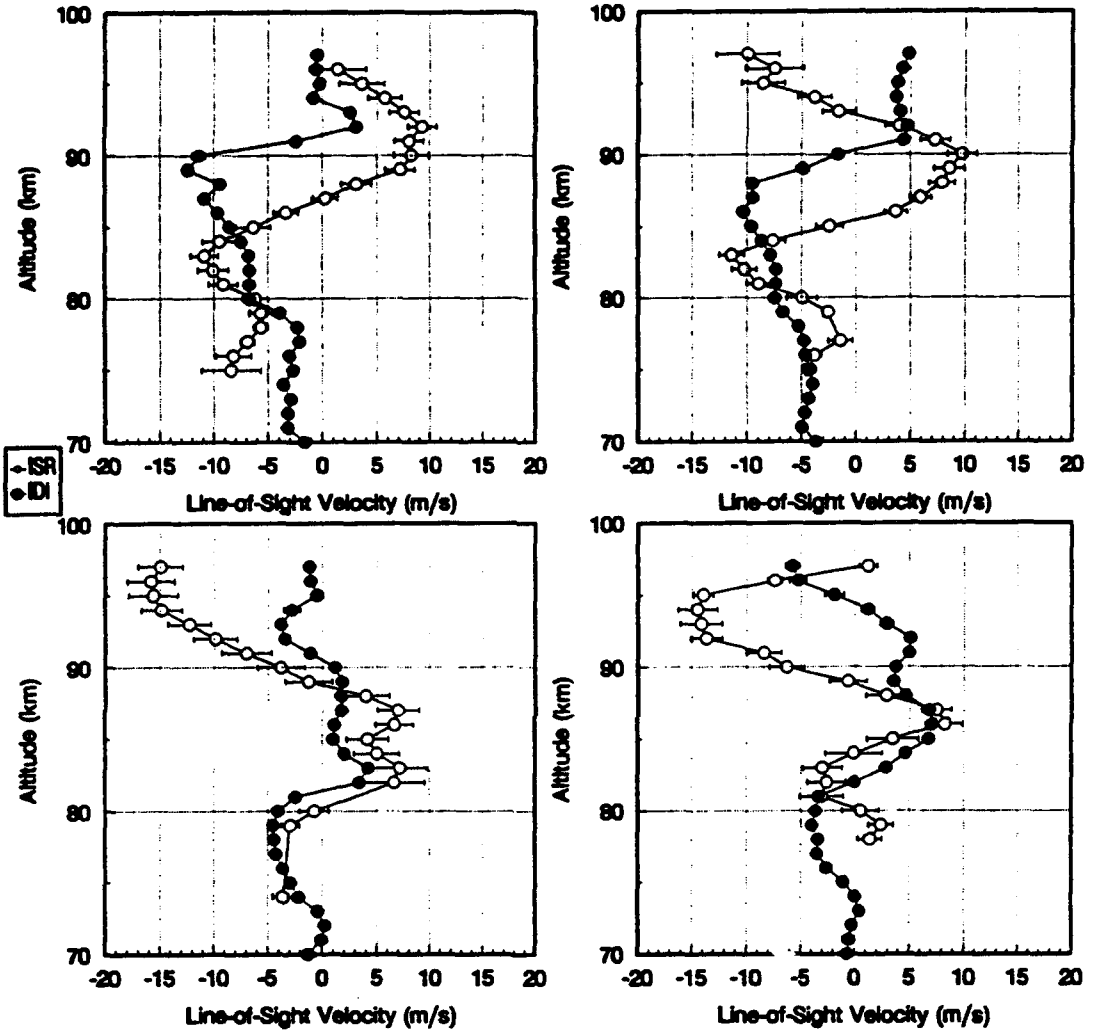
ISR
IDI
Altitude (km)
Line-of-Sight Velocity (m/s)
100
90
80
70
-20
-15
-10
-5
0
5
10
15
20

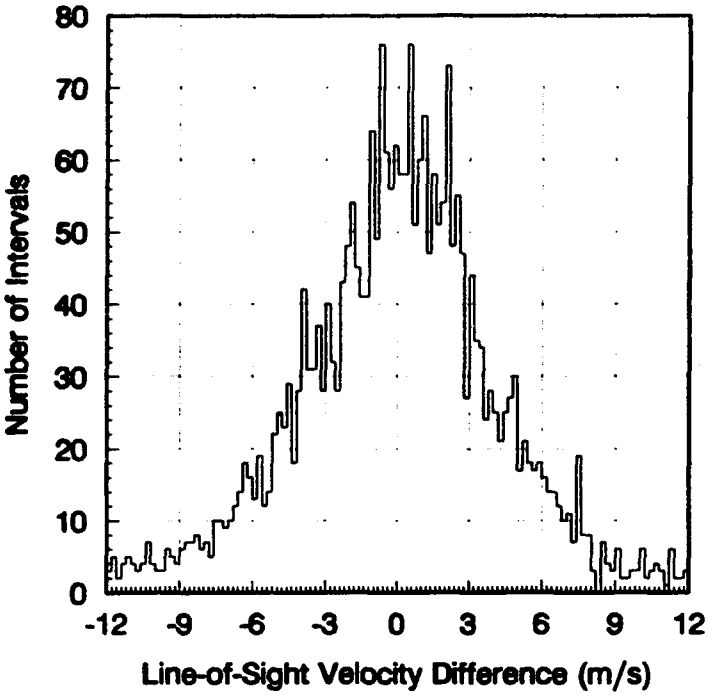
Number of Intervals
80
70
60
50
40
30
20
10
0
-12
-9
-6
-3
0
3
6
9
12
Line-of-Sight Velocity Difference (m/s)

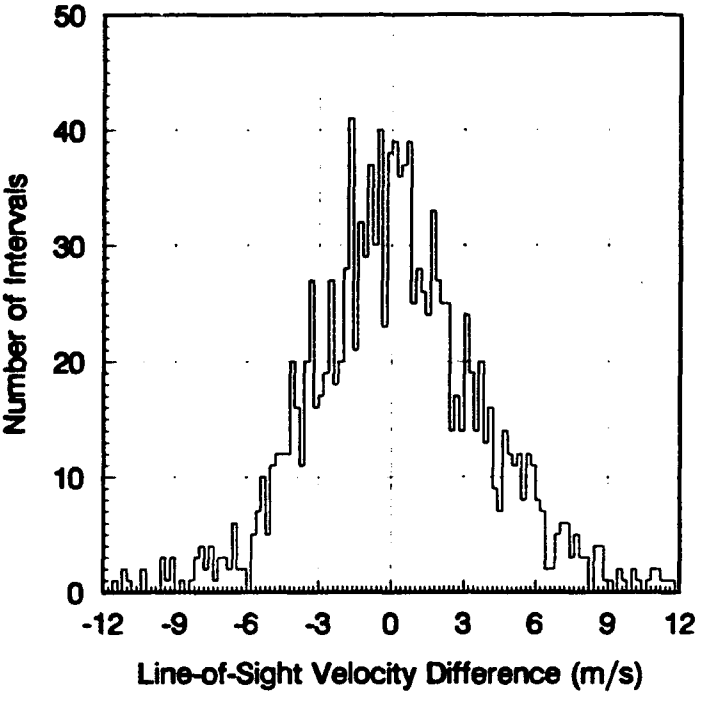
Number of Intervals
50
40
30
20
10
0
-12
-9
-6
-3
0
3
6
9
12
Line-of-Sight Velocity Difference (m/s)

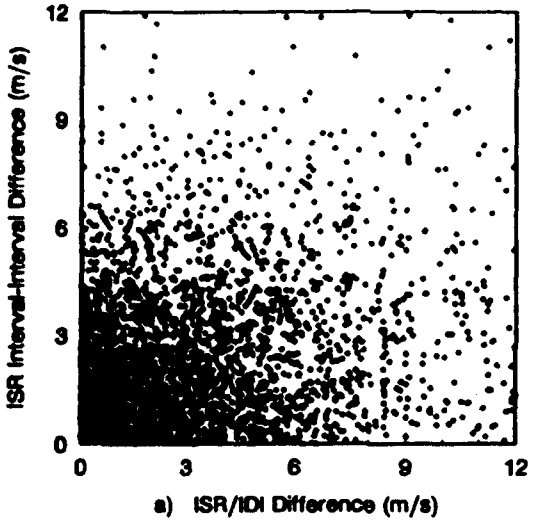
ISR Interval-Interval Difference (m/s)
0
3
6
9
12
a) ISR/IDI Difference (m/s)

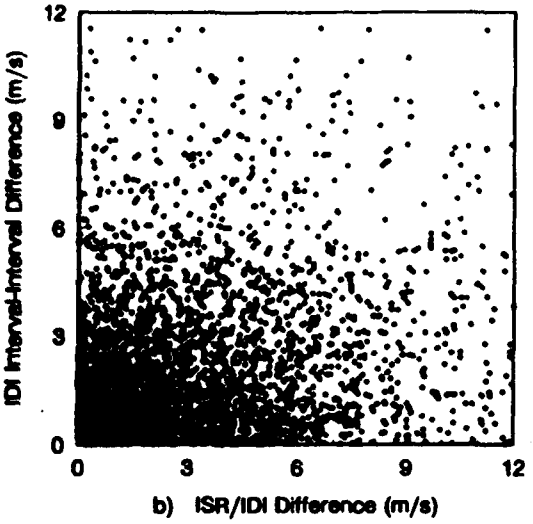
IDI Interval-Interval Difference (m/s)
0
3
6
9
12
b) ISR/IDI Difference (m/s)

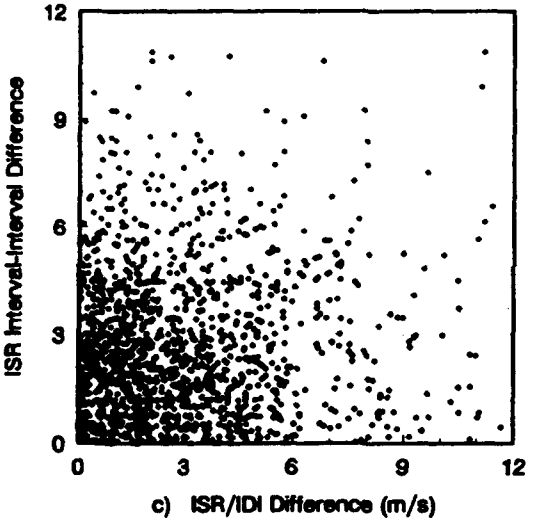
ISR Interval-Interval Difference
0
3
6
9
12
c) ISR/IDI Difference (m/s)

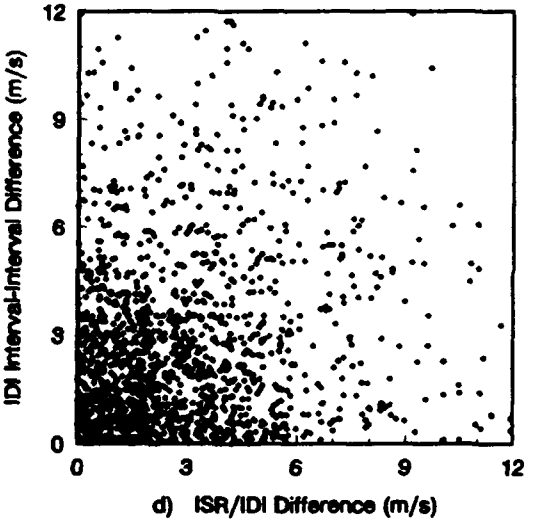
IDI Interval-Interval Difference (m/s)
0
3
6
9
12
d) ISR/IDI Difference (m/s)

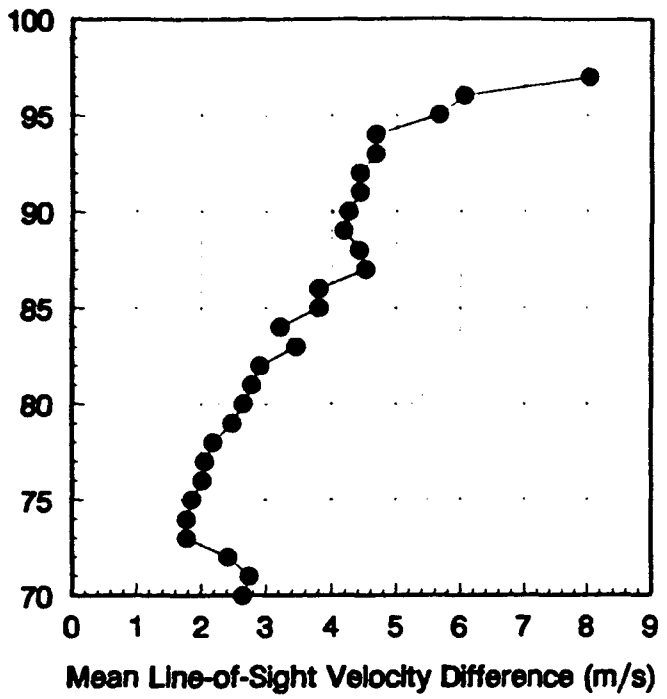
Altitude (km)
100
95
90
85
80
75
70
0 1 2 3 4 5 6 7 8 9
Mean Line-of-Sight Velocity Difference (m/s)

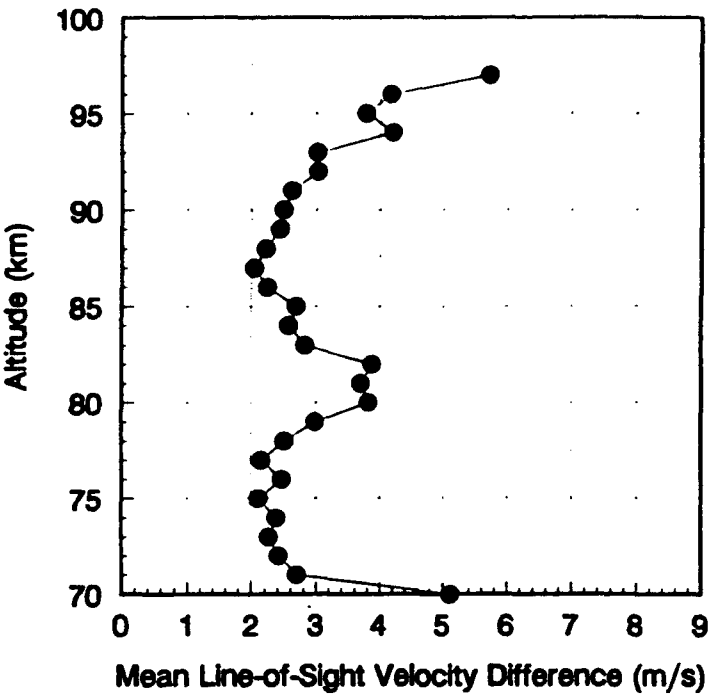
Altitude (km)
100
95
90
85
80
75
70
0 1 2 3 4 5 6 7 8 9
Mean Line-of-Sight Velocity Difference (m/s)

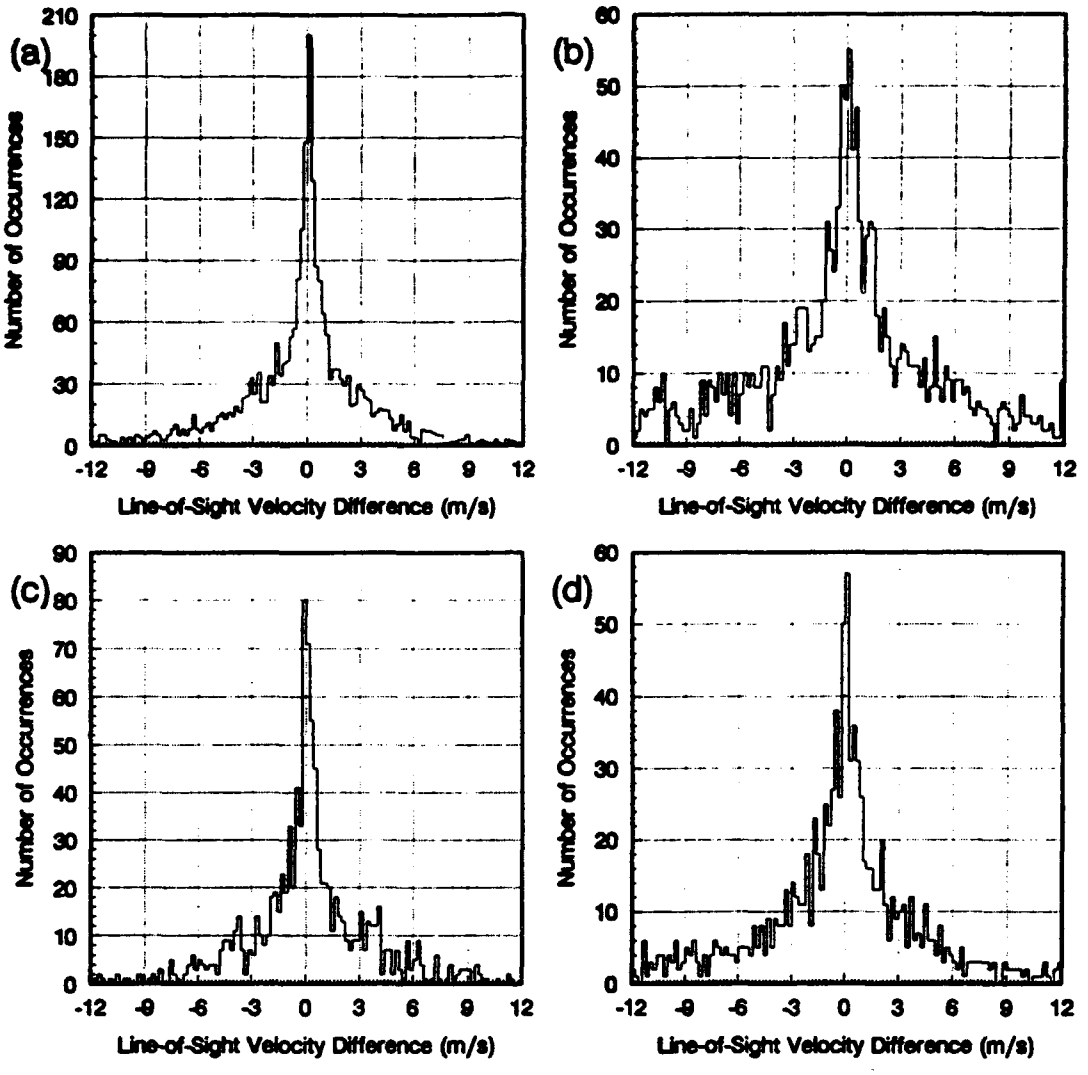
(a)
Number of Occurrences
Line-of-Sight Velocity Difference (m/s)
(b)
Number of Occurrences
Line-of-Sight Velocity Difference (m/s)
(c)
Number of Occurrences
Line-of-Sight Velocity Difference (m/s)
(d)
Number of Occurrences
Line-of-Sight Velocity Difference (m/s)

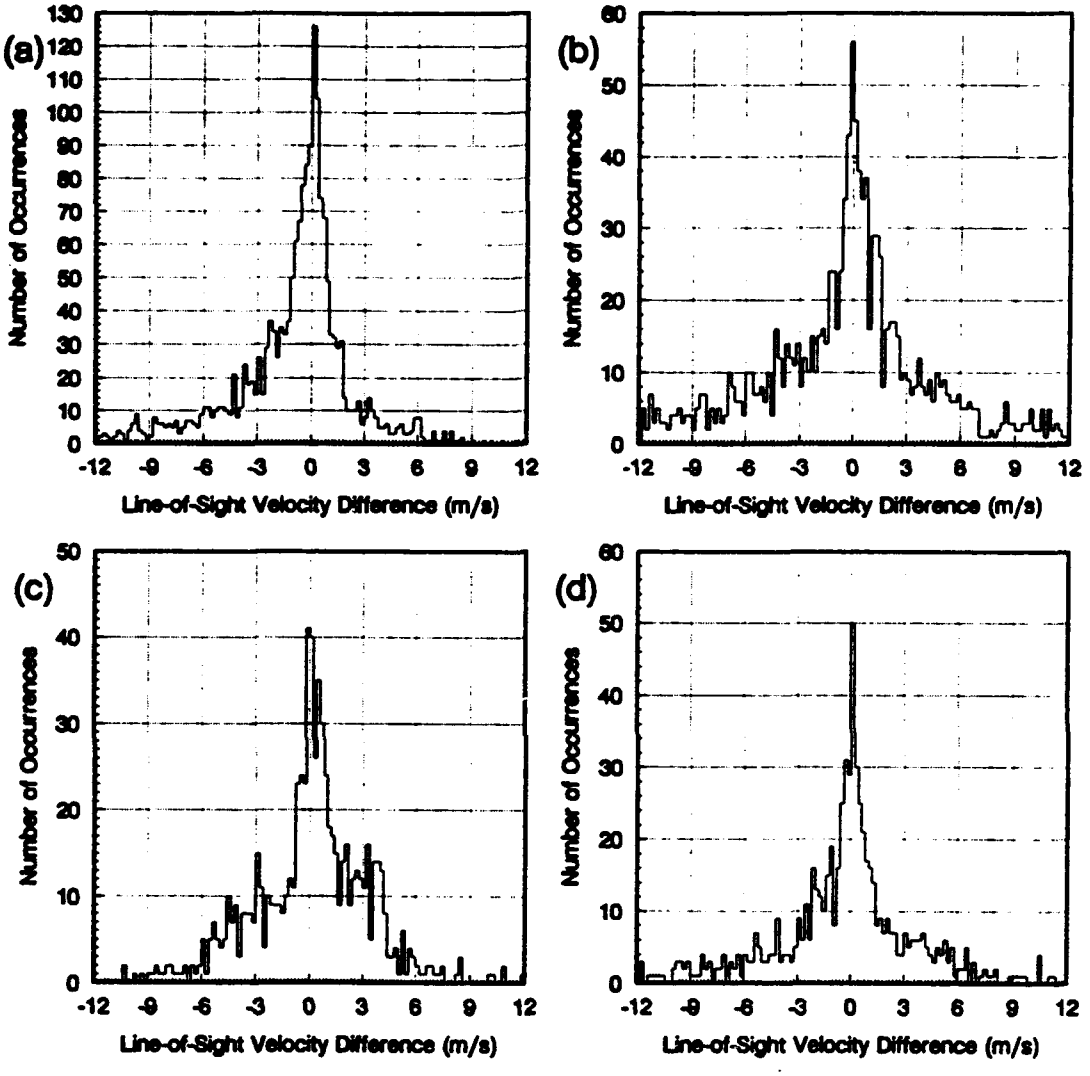
(a)
Number of Occurrences
Line-of-Sight Velocity Difference (m/s)
(b)
Number of Occurrences
Line-of-Sight Velocity Difference (m/s)
(c)
Number of Occurrences
Line-of-Sight Velocity Difference (m/s)
(d)
Number of Occurrences
Line-of-Sight Velocity Difference (m/s)

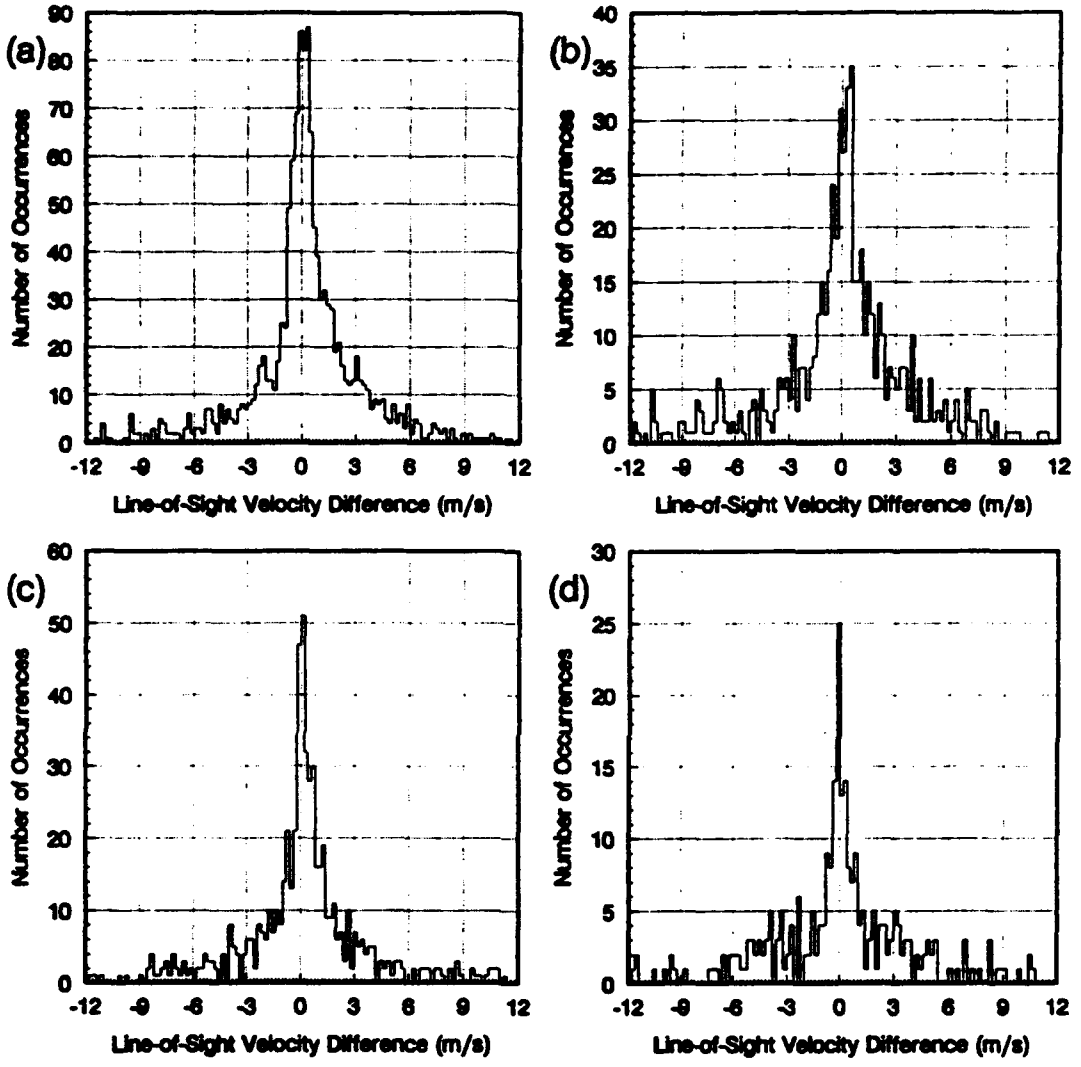
(a)
Number of Occurrences
Line-of-Sight Velocity Difference (m/s)
(b)
Number of Occurrences
Line-of-Sight Velocity Difference (m/s)
(c)
Number of Occurrences
Line-of-Sight Velocity Difference (m/s)
(d)
Number of Occurrences
Line-of-Sight Velocity Difference (m/s)

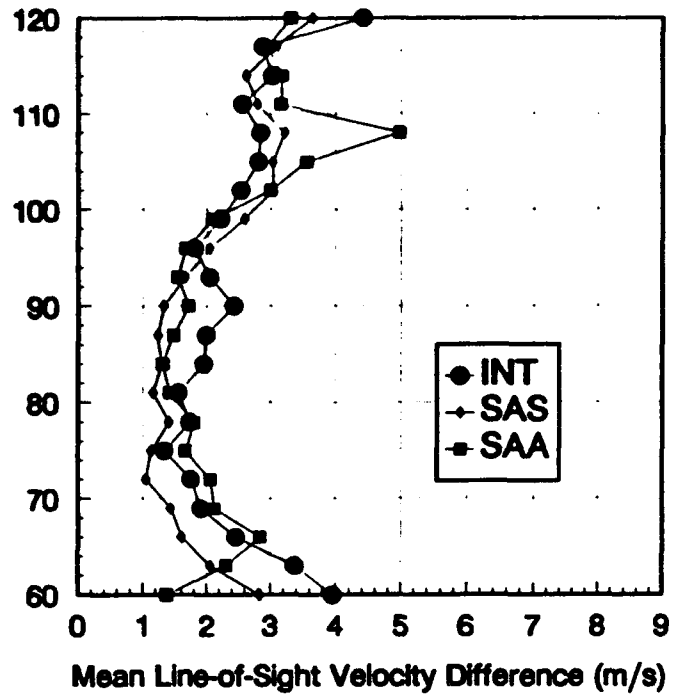
120
110
100
90
80
70
60
Altitude (km)
0 1 2 3 4 5 6 7 8 9
Mean Line-of-Sight Velocity Difference (m/s)
INT
SAS
SAA

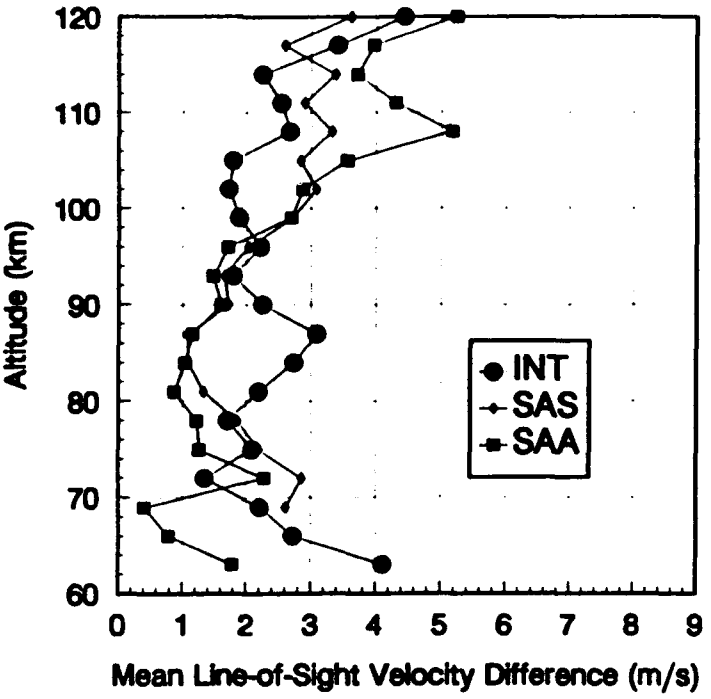
120
110
100
90
80
70
60
Altitude (km)
0 1 2 3 4 5 6 7 8 9
Mean Line-of-Sight Velocity Difference (m/s)
INT
SAS
SAA

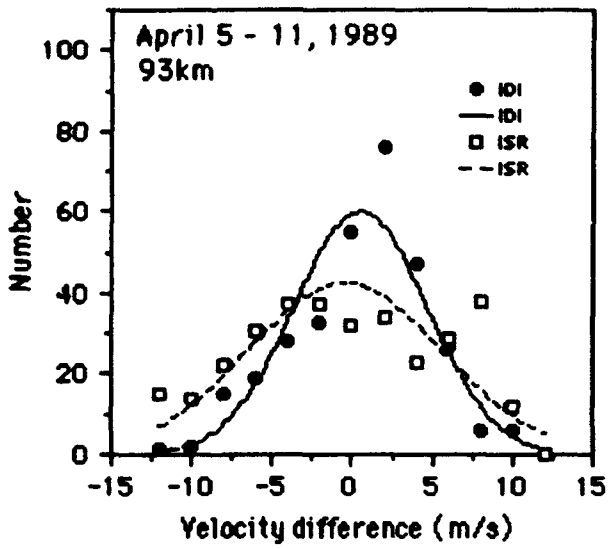
April 5 - 11, 1989
93km
IDI
IDI
ISR
ISR
Number
Velocity difference (m/s)

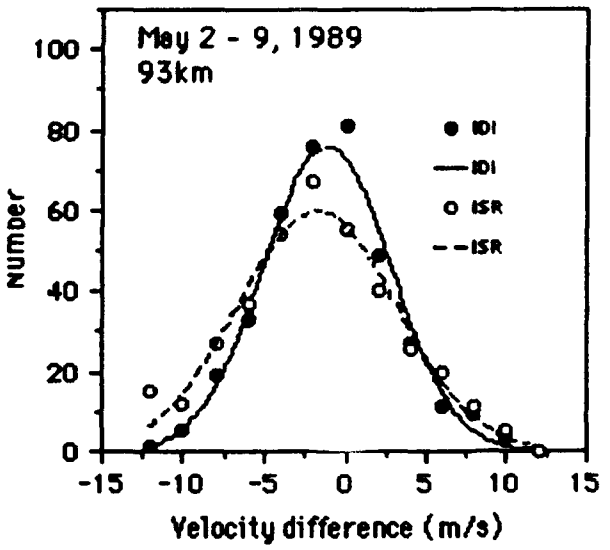
May 2 - 9, 1989
93km
IDI
IDI
ISR
ISR
Number
Velocity difference (m/s)

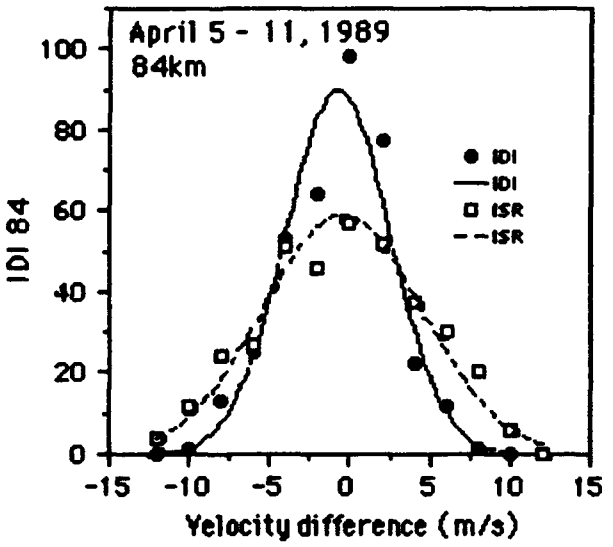
April 5 - 11, 1989
84km
IDI
IDI
ISR
ISR
IDI 84
Velocity difference (m/s)

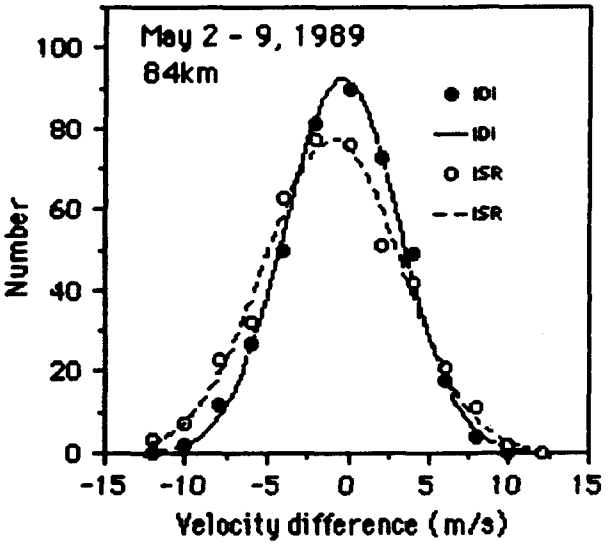
May 2 - 9, 1989
84km
IDI
IDI
ISR
ISR
Number
Velocity difference (m/s)

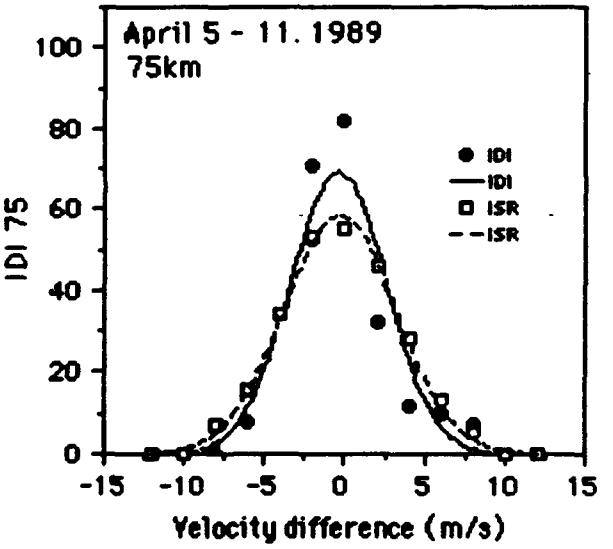
April 5 - 11. 1989
75km
IDI
IDI
ISR
ISR
IDI 75
Velocity difference (m/s)

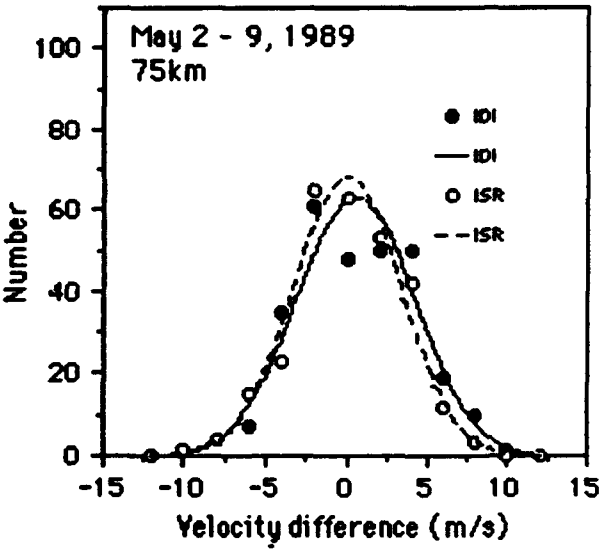
May 2 - 9, 1989
75km
IDI
IDI
ISR
ISR
Number
Velocity difference (m/s)

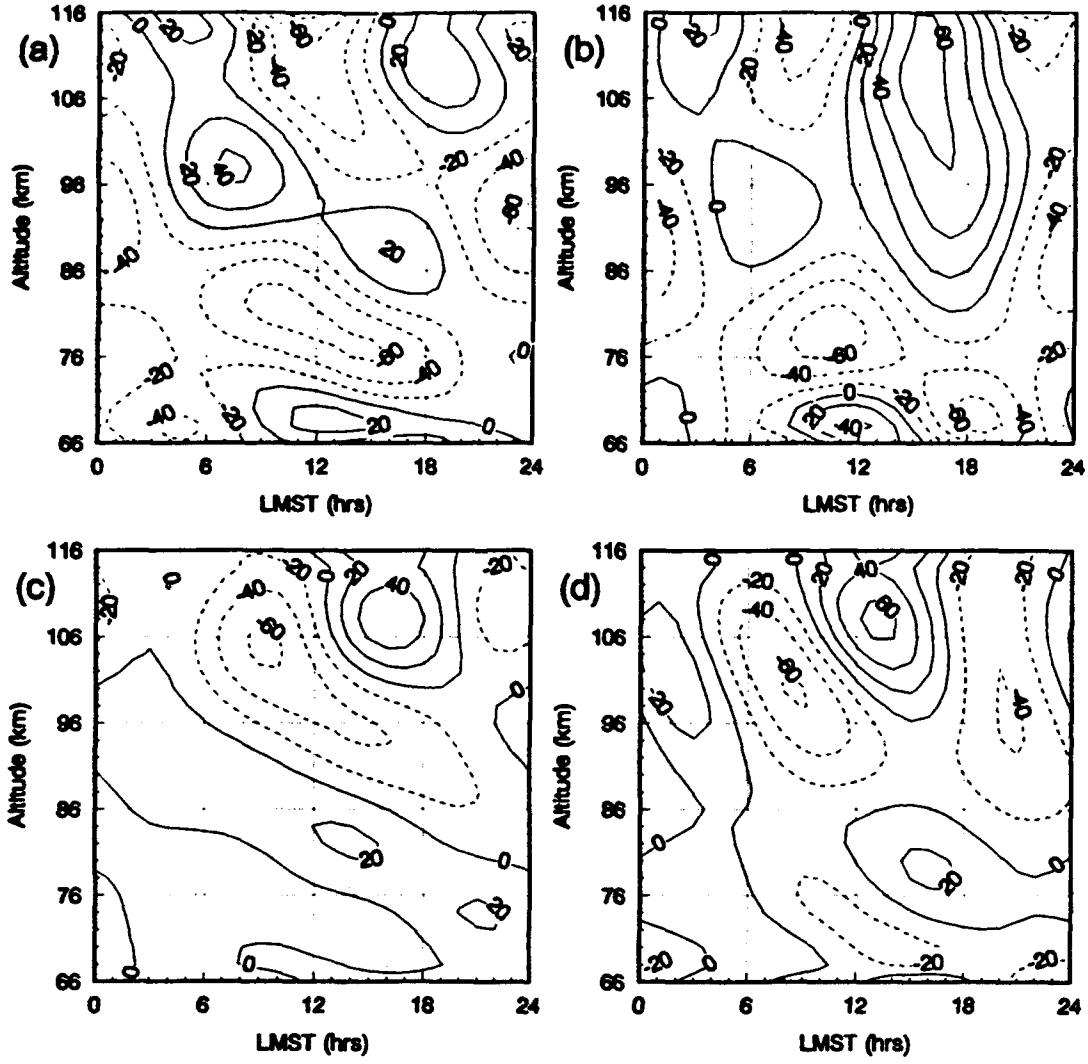
(a)
(b)
(c)
(d)
Altitude (km)
LMST (hrs)
116
106
96
86
76
66
0
6
12
18
24

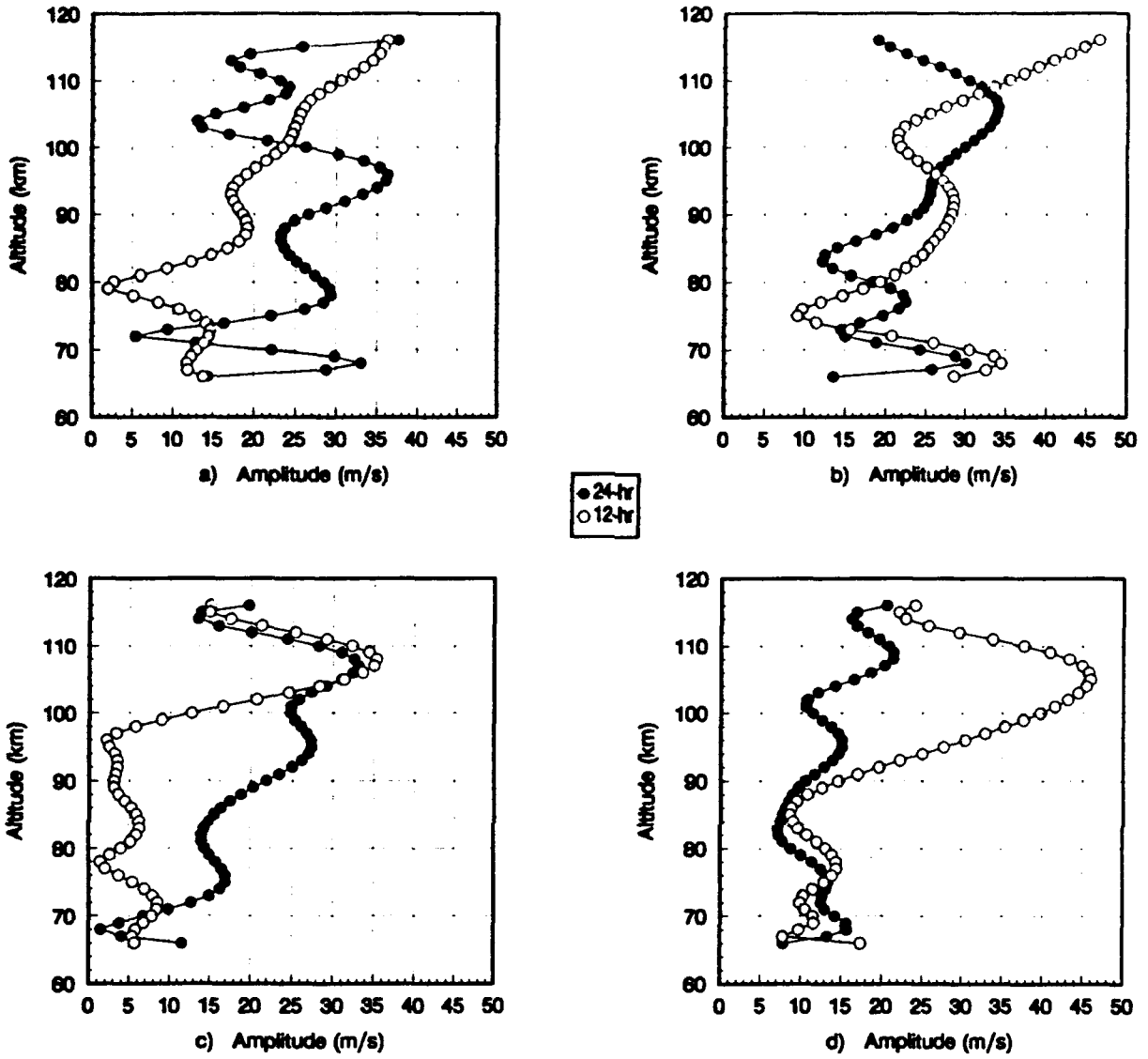
Altitude (km)
120
110
100
90
80
70
60
0 5 10 15 20 25 30 35 40 45 50
a) Amplitude (m/s)
b) Amplitude (m/s)
c) Amplitude (m/s)
d) Amplitude (m/s)
24-hr
12-hr

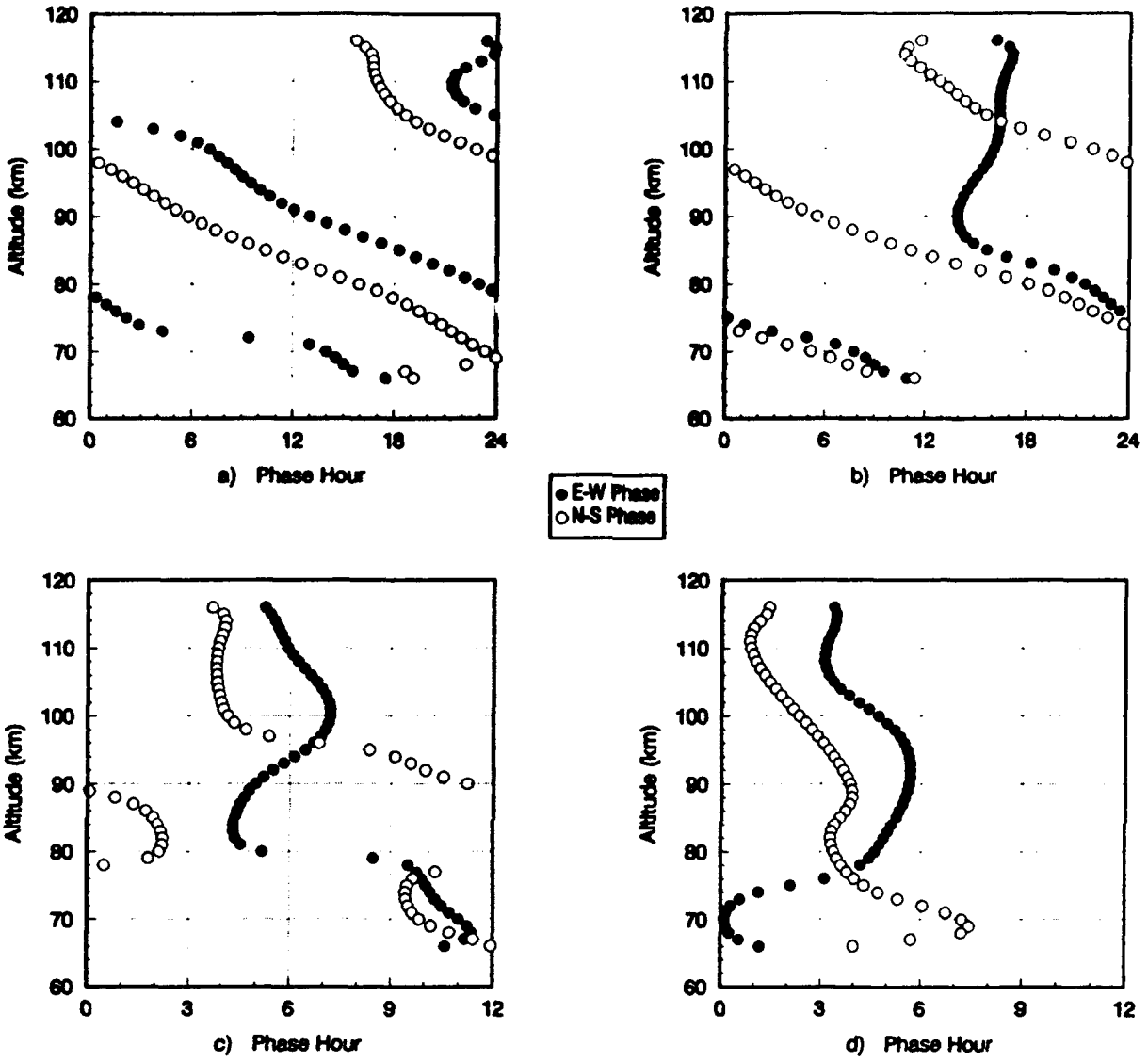
Altitude (km)
120
110
100
90
80
70
60
0
6
12
18
24
a) Phase Hour
b) Phase Hour
E-W Phase
N-S Phase
3
9
12
c) Phase Hour
d) Phase Hour

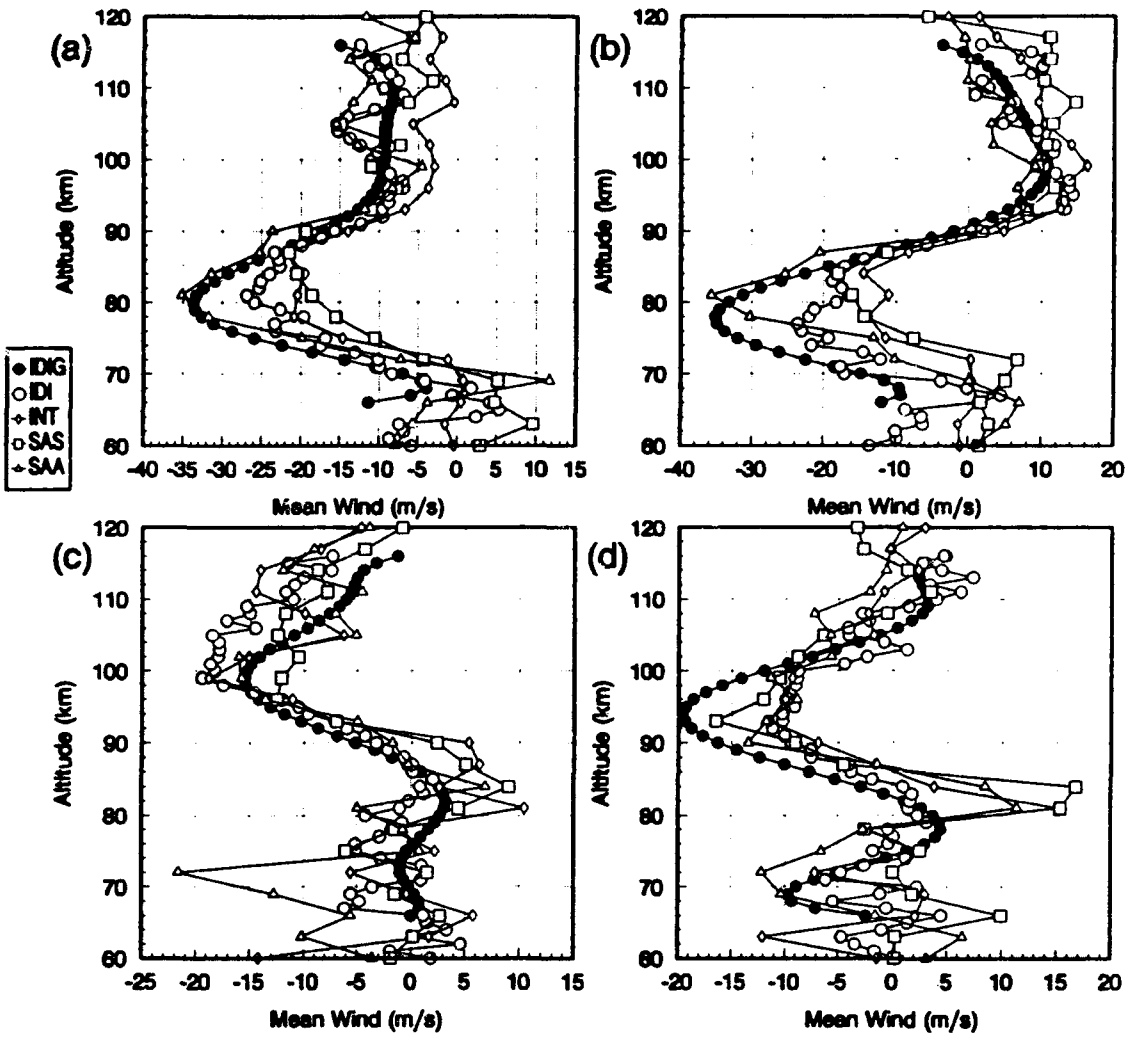
(a)
(b)
(c)
(d)
IDIG
IDI
INT
SAS
SAA
Altitude (km)
Mean Wind (m/s)

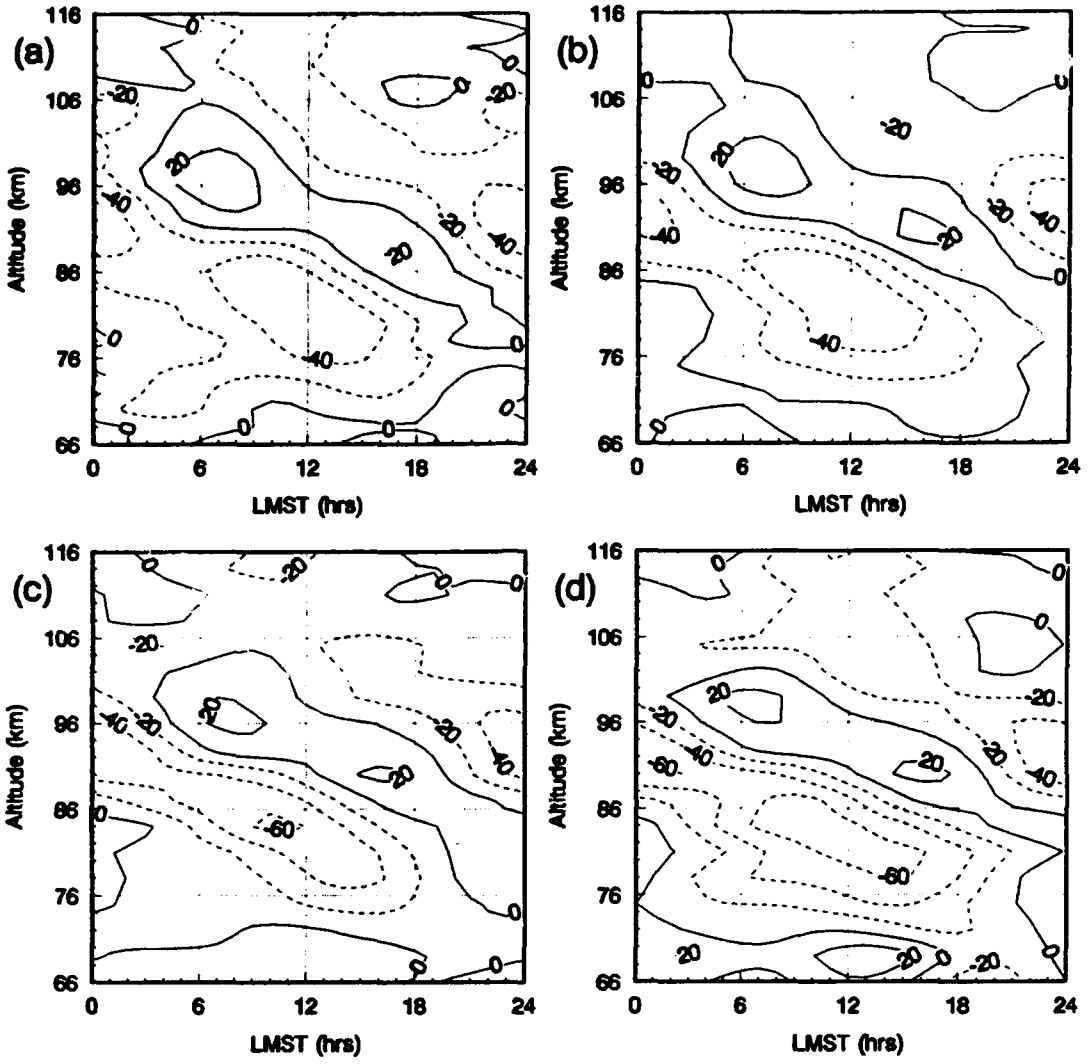
(a)
(b)
(c)
(d)
Altitude (km)
LMST (hrs)
116
106
96
86
76
66
0
6
12
18
24

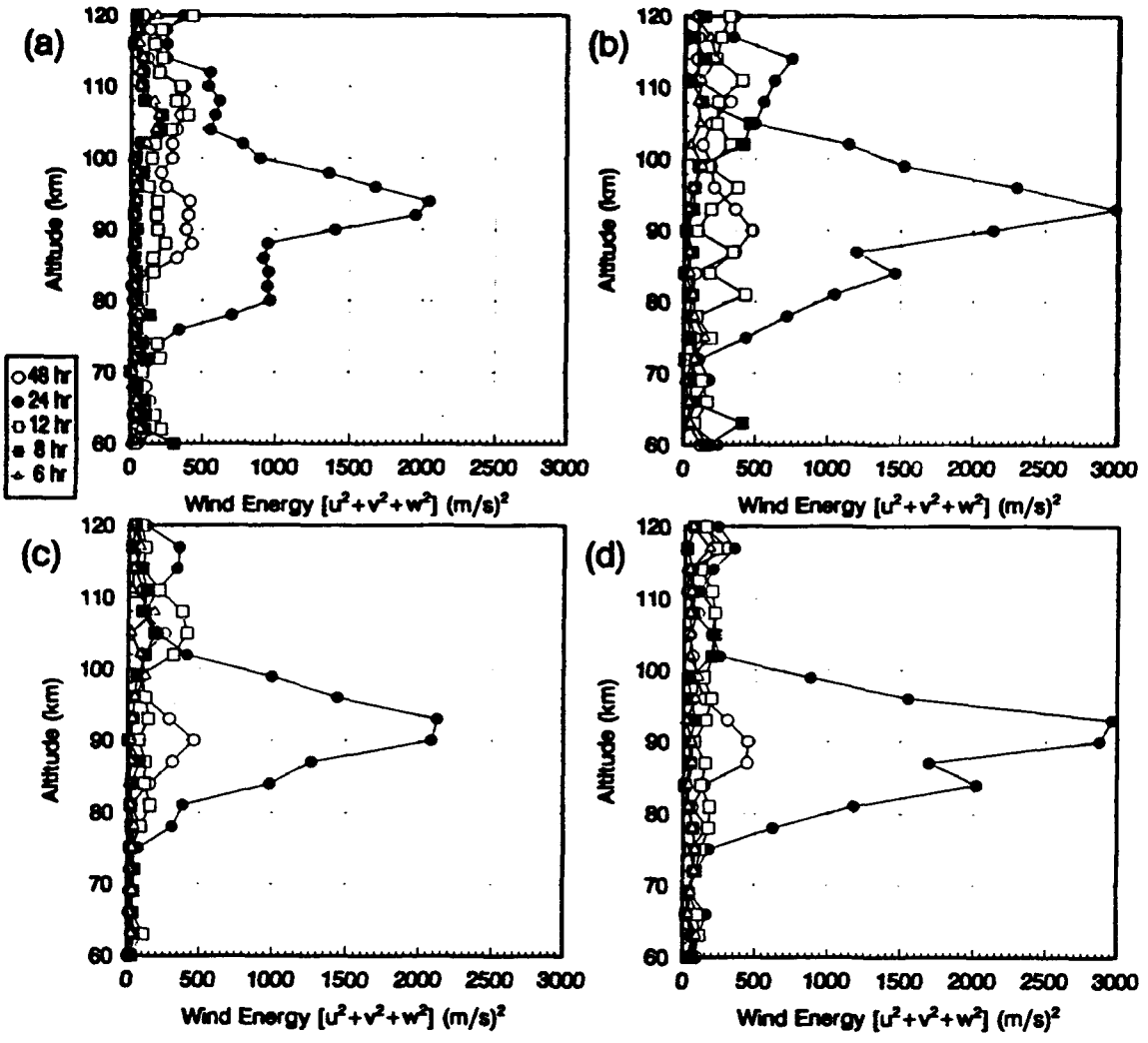
(a)
(b)
(c)
(d)
Altitude (km)
120
110
100
90
80
70
60
0
500
1000
1500
2000
2500
3000
Wind Energy [u²+v²+w²] (m/s)²
48 hr
24 hr
12 hr
8 hr
6 hr